REVIEW ARTICLE

Methods of single-molecule fluorescence spectroscopy and microscopy

W. E. Moerner[a] and David P. Fromm
Department of Chemistry, Stanford University, Mail Code 5080, Stanford, California 94305-5080

(Received 24 September 2002; accepted 21 April 2003)

Optical spectroscopy at the ultimate limit of a single molecule has grown over the past dozen years into a powerful technique for exploring the individual nanoscale behavior of molecules in complex local environments. Observing a single molecule removes the usual ensemble average, allowing the exploration of hidden heterogeneity in complex condensed phases as well as direct observation of dynamical state changes arising from photophysics and photochemistry, without synchronization. This article reviews the experimental techniques of single-molecule fluorescence spectroscopy and microscopy with emphasis on studies at room temperature where the same single molecule is studied for an extended period. Key to successful single-molecule detection is the need to optimize signal-to-noise ratio, and the physical parameters affecting both signal and noise are described in detail. Four successful microscopic methods including the wide-field techniques of epifluorescence and total internal reflection, as well as confocal and near-field optical scanning microscopies are described. In order to extract the maximum amount of information from an experiment, a wide array of properties of the emission can be recorded, such as polarization, spectrum, degree of energy transfer, and spatial position. Whatever variable is measured, the time dependence of the parameter can yield information about excited state lifetimes, photochemistry, local environmental fluctuations, enzymatic activity, quantum optics, and many other dynamical effects. Due to the breadth of applications now appearing, single-molecule spectroscopy and microscopy may be viewed as useful new tools for the study of dynamics in complex systems, especially where ensemble averaging or lack of synchronization may obscure the details of the process under study. [DOI: 10.1063/1.1589587]

I. INTRODUCTION

Single-molecule spectroscopy (SMS) allows *exactly one* molecule hidden deep within a condensed phase sample to be observed by using tunable optical radiation [Fig. 1(a)]. This represents detection and spectroscopy at the ultimate sensitivity level of $\sim 1.66\times 10^{-24}$ moles of the molecule of interest (1.66 yoctomole), or a quantity of moles equal to the inverse of Avogadro's number (a ''guacamole'').[1] To probe the molecule, a light beam (typically a laser) is used to pump an electronic transition of the one molecule resonant with the optical wavelength [Fig. 1(a)], and the resulting optical absorption is detected either directly[2] or indirectly by fluorescence excitation.[3] Detection of the single molecule of interest must be done in the presence of billions to trillions of solvent or host molecules and in the presence of noise from the measurement itself. The field of SMS has grown over the past dozen years to the status of a powerful technique for exploring the individual nanoscale behavior of molecules in complex local environments.[4,5]

How can SMS provide new information? Clearly, standard ensemble measurements which yield the average value of a parameter for a large number of (presumably identical) copies of the molecule of interest still have great value. By contrast, SMS completely removes the ensemble averaging, which allows construction of a frequency histogram of the actual distribution of values (i.e., the probability distribution function) for an experimental parameter. It is clear that the distribution contains more information than the average value alone. For example, the shape of the full distribution (indeed all the moments of the distribution) can be examined to see if it has multiple peaks, or whether it has a strongly skewed shape. Such details of the underlying distribution become crucially important when the system under study is heterogeneous. This would be expected to be the case for many complex condensed phase environments such as real crystals, polymers, or glasses. Fortunately, a single molecule can be a local reporter of its ''nanoenvironment,'' that is, of the exact constellation of functional groups, atoms, ions, electrostatic charges and/or other sources of local fields in its immediate vicinity. For biomolecules, heterogeneity easily arises, for example, if the various individual copies of a protein or oligonucleotide are in different folded states, different configurations, or different stages of an enzymatic cycle.

Another advantage of SMS measurements is that they remove the need for synchronization of many single molecules undergoing a time-dependent process. For example, a

[a]Author to whom correspondence should be addressed; electronic mail: wmoerner@stanford.edu

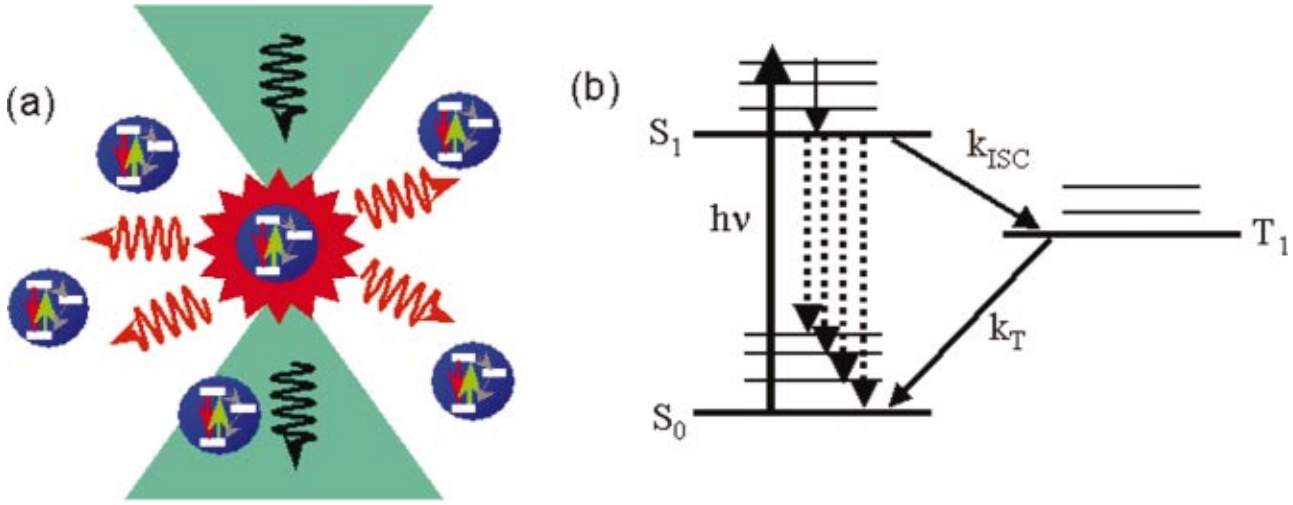

FIG. 1. (Color) (a) Schematic of an optical beam focal region (triangles) pumping a single resonant molecule, which subsequently either removes photons from the pumping beam or emits fluorescence. (b) Typical energy level scheme for single-molecule spectroscopy. S_0, ground singlet state; S_1, first excited singlet; T_1, lowest triplet state or other intermediate state. For each electronic state, several levels in the vibrational progression are shown. Pump photons at energy hν excite the dipole-allowed singlet–singlet transition. The intersystem crossing or intermediate production rate is k_{ISC}, and the triplet decay rate is k_T. Fluorescence emission shown as dotted lines originates from S_1 and terminates on various vibrationally excited levels of S_0 or S_0 itself.

large ensemble of molecules undergoing intersystem crossing events must be synchronized in order to measure the triplet lifetime, and this synchronization is only complete at the initial instant. Similarly, an enzymatic system may be in one of several catalytic states, and in an ensemble measurement initial synchronization is required but is quickly lost as the subsequent dynamical transitions of the individual enzymes are stochastic and generally uncorrelated. However, if single copies are observed, any one member of the ensemble is in only one state at a given time, and thus the specific sequence of state changes arising from binding, hydrolysis, and other catalytic steps is available for study. With proper time resolution, rare intermediates can be directly probed, whereas in the ensemble regime these fleeting species are in low concentration and can be swamped by other, more populated species. Using polarized excitation and/or polarization analysis of emission, the orientation of a molecular transition dipole can be used to follow mechanical changes such as the motion of biomolecular motors during the force generation process.

A final reason for the use of single-molecule techniques is the possibility of observing new effects in unexplored regimes. For example, several single-molecule systems have unexpectedly shown some form of fluctuating, flickering, or stochastic behavior.[6] The absorption frequency of the single molecule can change as a result a change in its photophysical parameters or a change in local environment; this behavior has been termed ''spectral diffusion,'' and it can produce spectral shifts or fluctuations. Such fluctuations are now becoming important diagnostics of the single-molecule regime, and they provide unprecedented insight into behavior which is generally obscured by ensemble averaging. On a fundamental level, the time-dependent dynamical behavior of an individual quantum system would be expected to show ''quantum jumps'' [7] as transitions between states occur, and this can be directly observed by SMS techniques.[8]

Stepping back for a moment, the last few decades have witnessed a dramatic increase in interest in the ''nanoworld'' of single atoms, ions, and molecules, for both scientific and technological reasons. Indeed, SMS as defined is related to, but distinct from, several recently successful lines of research on individual species: (i) the spectroscopy of single electrons or ions confined in electromagnetic traps;[9–11] (ii) scanning tunneling microscopy,[12] and atomic force microscopy[13] of atoms and molecules on surfaces; (iii) the study of ion currents in single transmembrane channels;[14] (iv) single polymer or DNA chains with high concentrations of fluorophores;[15] and (v) force measurements on single molecular motors using optical traps.[16,17]

It is useful to note that at room temperature and under appropriate dilution conditions one can detect the burst of emitted photons as a single fluorescent molecule in flowing solution passes through the focus of a laser beam.[18–21] This area was pioneered by the Keller group at Los Alamos, and has been the subject of a recent monograph.[22] A related technique, fluorescence correlation spectroscopy (FCS), uses Brownian motion to bring single molecules through a focused laser spot. By calculating the autocorrelation of the emitted bursts of light, time-dependent dynamics can be followed in detail.[23–29] However, since the emission bursts from many single molecules are summed in the autocorrelation, differences between individuals may be hard to detect. In this article, the focus is on microscopic imaging methods, where one observes the same single molecule for an extended period (longer than the diffusion time through the laser focus), measuring signal strength, lifetime, polarization, fluctuations, and so on, all as a function of time. Nevertheless, the analyses of signal, noise, background, and detection considerations presented in Sec. II below apply directly to detection problems in flowing streams and FCS as well.

At present, the impact of SMS spans several fields, from physics, to chemistry, to biology, and the number of applications continues to expand. In this article, the primary experimental techniques for single-molecule fluorescence detection

and microscopy at room temperature will be reviewed. After a summary of the basic principles controlling the signal-to-noise ratio, a variety of microscopic configurations will be described. This will be followed by a short description of many of the detection modalities that have been developed in order to extract information from a single-molecule optical experiment. Several comprehensive reviews of this area may be consulted for details of the scientific results that have been obtained by researchers around the world.[4,5,21,22,30–40]

II. BASIC PRINCIPLES

How is it possible to use optical radiation to isolate and probe a single impurity molecule on a surface, in a liquid, or inside a solid sample? To answer this question concisely, single-molecule optical spectroscopy is accomplished by two deceptively simple steps: (a) guaranteeing that only one molecule is in resonance in the volume probed by the laser, and (b) providing a signal-to-noise ratio (SNR) for the single-molecule signal that is greater than unity for a reasonable averaging time. These two requirements will now be treated briefly, and then in more detail.

At room temperature, guaranteeing that only one molecule is in resonance is generally achieved by a combination of focusing the laser to a small probe volume ($\sim 1-100\ \mu m^3$, even down to $10^{-4}\ \mu m^3$ for near-field methods), using an ultrapure host matrix, and selecting an ultralow concentration of the impurity molecule of interest. The concentration required depends upon the volume probed by the pumping laser, which varies somewhat depending on the technique and the sample under study as described in more detail below. For example, at room temperature one need only work with roughly 10^{-10} mole/L concentration in a probed volume of 10 μm^3 to achieve the limit of one molecule in resonance. At liquid helium temperatures, the phenomenon of inhomogeneous broadening[41–43] can be used to achieve dilution factors from $\sim 10^4-10^5$ simply by tuning the laser frequency to a spectral region where only one molecule is in resonance.[30,38] This spectral selection technique was crucial to the first demonstrations of SMS.[2,3] As this article concentrates on room temperature methods, the detailed considerations[33,44,45] that apply to low temperature spectral selection techniques will not be described further. A cartoon of the selection process is shown in Fig. 1(a), where a focused laser beam selects only one molecule and SMS is achieved by detection of the photons from this molecule.

Achieving the required SNR requires close attention to maximizing signal while minimizing backgrounds and the relative size of laser shot noise. To obtain as large a signal as possible, one needs a combination of small focal volume, large absorption cross section, high photostability, weak bottlenecks into dark states such as triplet states, and operation below saturation of the molecular absorption. For fluorescence methods, one must select an impurity molecule with the highest fluorescence quantum efficiency as possible. In addition, one must rigorously exclude undesirable fluorescent impurities, minimize the volume probed to reduce Raman scattering, and scrupulously reject any Rayleigh scattered radiation at the pumping wavelength. For absorption methods, achieving a low noise level from nonideal effects follows from careful reduction of residual signals and operation at a power level sufficient to reduce the relative contribution from laser shot noise, see Refs. 30, 44, and 46 for details.

A. Signal size

The signal of interest here arises from the fluorescent photons emitted by the single molecule. While the number of photons emitted per second for one molecule is far smaller than the number of photons per second in the incident laser beam, the fact that the emitted photons are generally redshifted to longer wavelengths enables detection with reasonable SNR. Figure 1(b) shows the salient features of the most common energy level structure of molecules that have been explored by SMS. The molecule has an electric–dipole-allowed singlet–singlet optical transition $S_1 \leftarrow S_0$, pumped by radiation at energy $h\nu$ from a laser or a lamp, with h the Planck constant and ν the optical frequency. It is generally not necessary to pump the lowest electronic excited state, so absorption into a vibrationally excited sideband is sufficient. After the absorption of the pump photon, the excited molecule quickly relaxes by emission of vibrational modes of the molecule (intramolecular vibrational relaxation) and of the host (phonons) to the lowest electronic excited state, from which fluorescence photons can be emitted (dashed lines). (There is also a certain probability for intersystem crossing into the triplet state manifold temporarily, *vide infra*.) After the emission, the molecule is brought back to the initial ground state by further vibrational and phonon relaxation, and the partitioning between the various colors of emission is controlled by the well-known Franck–Condon and Debye–Waller factors expressing the extent of vibrational relaxation and electron–phonon coupling, respectively. In general, the relaxation steps represent energy losses which cause a spectral redshift between absorption and emission bands, called the Stokes shift. Typical fluorescent molecules used for SMS come from the general classes of laser dyes used in biological fluorescent labeling (rhodamines, cyanines, oxazines, etc.),[47] rigid aromatic hydrocarbons such as terrylene,[48] or perylene diimides,[49,50] as well as autofluorescent, genetically expressed proteins such as the green fluorescent protein (GFP) and its relatives.[51,52] Some proteins are naturally fluorescent due to presence of one or many fluorophores as cofactors, and these have also provided useful single-molecule signals in the cases of flavoenzymes[53,54] and antenna complexes containing bacteriochlorophyll molecules.[55] In recent work, a new class of single-molecule fluorophores has been found among molecules originally optimized for nonlinear optical properties.[56] The degree of redshift of the emission varies, but the laser dyes for example often undergo large rearrangements of their charge distribution upon excitation, leading to much larger Stokes shifts (about 1500 cm^{-1} for rhodamine dyes, 6000 cm^{-1} for DCM, another well-known laser dye) than for aromatic hydrocarbons. Strong fluorescence has also been observed for single semiconductor quantum dots,[57] and these emitters have been proposed as biological labels.[58] This approach requires methods for attachment of the dots to biomolecules, an area of intense current re-

search. From the photophysical point of view, these fascinating emitters behave like two-level systems on short time scales,[59] have narrow emission lines and resist photobleaching, yet show fluorescence intermittency and blinking over many decades in time.[60,61]

To maximize the fluorescence emission rate, it is necessary to pump the molecule with high probability and to have the largest possible fluorescence quantum yield ϕ_F. For focal spots of area greater than or equal to the diffraction-limited value (approximately $(\lambda/2)^2$, with λ the optical wavelength), the rate at which the resonant optical transition is pumped is given by the product of the incident photon flux [in photons/(s cm^2)] and the absorption cross section σ_p (in cm^2). Stated differently, the probability that a single molecule will absorb an incident photon from the pumping laser beam is just σ_p/A, where A is the cross-sectional area of the focused laser beam. Thus, σ_p may be interpreted as the effective ''area'' (per molecule) which is able to ''capture'' photons from the incident laser beam. High σ_p means that the photons of the incident light beam are efficiently absorbed and therefore background signals from unabsorbed photons are minimized compared to the case for weak absorbers. Thus it comes as no surprise that maximizing the absorption cross section is crucial to the detection of single molecules.

Generally, the maximum values of σ_p arise from strongly allowed electric dipole transitions, and the value of this quantity is intimately connected to the quantum-mechanical details of the electronic transition, specifically to the transition dipole moment (or equivalently, the radiative rate given by the Einstein A coefficient). The general expression for the (peak) cross section for a randomly oriented molecule is

$$\sigma_p = 2\pi(\lambda/2\pi)^2(\gamma_r/\Gamma_{\mathrm{tot}}), \tag{1}$$

where λ is the light wavelength, γ_r the spontaneous (that is, radiative) fluorescence rate, and Γ_{tot} the total frequency width of the absorption.[4,44,62] Happily, most electric–dipole-allowed transitions in organic molecules have oscillator strengths on the order of unity. For a dye molecule in solution at room temperature with $\lambda = 500$ nm, γ_r is about 10^{-3} cm^{-1}, which corresponds to a radiative lifetime of a few ns, and Γ_{tot} is about 1000 cm^{-1}, so that the absorption cross section of a single dye molecule is $\sigma_p \sim 4$ Å$^2 = 4 \times 10^{-16}$ cm^2, a value comparable to the molecular size. A somewhat more convenient way to estimate the value of the absorption cross section at room temperature is to use the well-known connection between molecular extinction coefficient ε (units L mol^{-1} cm^{-1}, tabulated and easily measured) and the cross section[63]

$$\sigma = 2.303\varepsilon/N_A \tag{2}$$

in units cm^2, with N_A the Avogadro constant. [At low temperatures, optical absorption profiles become extremely narrow so that all molecules in the sample may not be resonant with the pumping laser, and more careful methods must be used to determine the cross section.[44,64] In this case, the total width of the absorption becomes so narrow that cross sections often approach the fundamental maximum value of $\lambda^2/(2\pi)$.][38]

The other key molecular parameter controlling the amount of emitted fluorescence is the probability for photon emission per absorption event, i.e., the fluorescence quantum yield ϕ_F. This parameter should clearly be high, as close to unity as possible. The fluorescence quantum yield is generally given by

$$\phi_F = k_{\mathrm{rad}}/(k_{\mathrm{rad}} + k_{\mathrm{nonrad}}) = \tau_F/\tau_{\mathrm{rad}}, \tag{3}$$

where k_{rad} is the radiative rate (Einstein A coefficient), k_{nonrad} is the sum of all nonradiative rates such as internal conversion or intersystem crossing, τ_F is the observed excited state lifetime (fluorescence lifetime), and τ_{rad} is the radiative lifetime.[63] Thus, the best fluorophores are those with relatively rigid structures so that the primary path for deactivation of the excited state is via the emission of a fluorescent photon. Molecules that twist or distort greatly in the excited state typically have non-negligible nonradiative decay channels. For a strong emitter (and absorber) like R6G where $\phi_F \sim 0.45$ (in water),[65] the fluorescence lifetime is ~ 4 ns. This means that if the molecule were a two-level system, the maximum emission rate would be on the order of 10^8 s^{-1}. Although this is quite a large signal, several effects act to limit the maximum photon emission rate and the maximum number of photons emitted, which will now be described.

The first physical effect that limits the maximum emission rate from a molecule is optical saturation of the transition. As laser power is increased, more and more photons are emitted per second, as long as the optical transition is not saturated. When saturation occurs, the absorption cross section from the molecule decreases, and further increases in laser power generate more background photons rather than signal photons. More precisely, the cross section for absorption depends upon pumping laser intensity I as

$$\sigma_P = \sigma_P^0/(1 + I/I_S), \tag{4}$$

where I_S is the characteristic saturation intensity. The saturation intensity depends upon further details of the energy level structure of the molecule. In the limit that the molecule approximates a two-level system, the saturation intensity is given by

$$I_S = h\nu/(2\sigma\tau_F). \tag{5}$$

This equation expresses the fact that if the rate of absorption of incident photons gets too high, the molecule cannot decay back to the ground state fast enough, thus the ability of the molecule to absorb photons decreases.

Although some fluorophores do approach the two-level limit, it is generally more appropriate to consider the three-level case shown in Fig. 1(b). The intersystem crossing process shown may be regarded as a model for any bottleneck that takes the molecule into a form that no longer absorbs or emits photons. In organic molecules, intersystem crossing (ISC) is seldom rigorously absent, and when ISC occurs, both absorption of photons and photon emission cease for a relatively long time equal to the triplet lifetime ($=1/k_T$). This effect results in premature saturation of the emission

rate from the molecule and reduction of the absorption cross section σ_p compared to the two-level case.[66] The saturation intensity for a molecule with a triplet bottleneck may be written[45,67]

$$I_S = \frac{h\nu}{2\sigma\tau_{21}}\left[\frac{1+(k_{\mathrm{ISC}}/k_{21})}{1+(k_{\mathrm{ISC}}/2k_T)}\right], \tag{6}$$

where $k_{21}=1/\tau_{21}$ is the rate of direct decay from S_1 to S_0, k_{ISC} is the rate of intersystem crossing, and k_T is the total decay rate from the lowest triplet T_1 back to S_0. Clearly, this more accurate saturation intensity is smaller than the two-level value by the bracketed factor on the right, and smaller saturation intensities mean the laser power that can be used to probe the system is limited (for fixed focal spot area).

The effect of saturation can be seen in both the peak on-resonance emission rate from the molecule $R(I)$ and in the single-molecule linewidth $\Delta\nu(I)$ by solving the three-level rate equations with the result[36,66]

$$R(I) = R_\infty\left[\frac{I/I_S}{1+I/I_S}\right], \tag{7}$$

$$\Delta\nu(I) = \Delta\nu(0)[1+(I/I_S)]^{1/2}, \tag{8}$$

where the maximum emission rate is given by

$$R_\infty = \frac{(k_{21}+k_{\mathrm{ISC}})\phi_{\mathrm{F}}}{2+(k_{\mathrm{ISC}}/k_T)}. \tag{9}$$

Equations (7) and (8) show that the integrated area under the single-molecule peak falls in the strong saturation regime. At the same time, at higher and higher laser power, more and more scattering signal is produced in (linear) proportion to the laser power, so the difficulty of detecting a single molecule increases. This specific effect will be explored more directly in the SNR discussion in Sec. III C. The dependences of the maximum emission rate and linewidth on laser intensity in Eqs. (7) and (8) have been verified experimentally for individual single molecules.[66] In summary, minimizing the triplet bottleneck means small values of k_{ISC} and large values of k_T, requirements which are satisfied for rigid, planar aromatic laser dye molecules, aromatic hydrocarbons, and other good fluorophores. In cases where the photophysical parameters of all bottleneck states are not known, it may be more convenient to directly measure the saturation intensity by recording and fitting the intensity-dependent transmission of a bulk sample to determine I_S.[68] In particular, for real molecules at room temperature, situations may occur where rapid relaxation and decoherence in the vibrational manifolds should be taken into account, and it may become necessary to go beyond the three-level model presented here.

A final physical effect that limits the (integrated) signal from a single molecule is photobleaching, a general term for any photochemical process that causes the molecule to eventually change to another form and stop absorbing and/or emitting photons. In practice, at room temperature almost all molecules in aqueous solution photobleach after the emission of $\sim 10^6$ photons. Specific values of the photobleaching quantum yield ϕ_B are provided, e.g., in Refs. 65 and 69; generally the maximum number of photons emitted on average is given by $1/\phi_B$. In many cases, photobleaching is actually a photo-oxidation of the fluorophore, so measures to reduce the presence of molecular oxygen can help in minimizing this effect. Successful methods have involved: (a) the use of an enzymatic oxygen scavenger system,[70,71] (b) flooding the sample with an inert gas such as argon or nitrogen,[72] and (c) operating in vacuum.[73]

B. Background issues

To detect a single molecule, one must simultaneously maximize signal while at the same time scrupulously minimize background photons, noise from unwanted sources, and detector dark counts. For the purposes of this discussion, ''noise'' refers to fluctuations arising from effects such as Poisson statistics of detected photons, while ''background'' refers to photons that may arrive at the detector from any source other than the single molecule of interest. Background signals generally scale linearly with the pumping laser power, while detector dark counts do not.

In spite of much effort to reduce backgrounds, almost all single-molecule fluorescence experiments are background limited and the shot noise of the probing laser is only important for the signal-to-noise of the spectral feature. Therefore, conquering background signals must be one of the primary goals of the single-molecule experimental design. A first source of background may result from experimental limitations such as the residual fluorescence from optical parts, particularly from colored glass filters or from the microscope objective itself. It is also possible to have residual emission from the excitation source in the red-shifted spectral range where fluorescence is detected. This source of background can be a critical issue when the laser in use is a diode laser, and multiple filters may be required to suppress laser emission to long wavelengths of the primary mode. In general, by careful selection of high-quality components, these sources of background may be minimized.

However, background photons arising from the sample itself are more difficult to suppress. These are of two types: elastic Rayleigh scattering of the laser wavelength, and photons that are red-shifted in wavelength into the spectral region of the single-molecule fluorescence and hence that can obscure the photons from the single molecule. Rayleigh-scattered pump radiation can be reduced by using ultraclean, scratch-free substrates of the highest quality and by the use of interference filters as described below. The two main sources of redshifted photons are residual fluorescence from other impurities, and Raman scattering by the solvent or host matrix. Both are proportional to the volume of the illuminated sample. Even if their fluorescence yield is very weak, unwanted impurities or molecular components of the host medium, particularly in biological samples, can emit strong residual fluorescence due simply to the fact that billions or trillions of host molecules may be present in the illuminated volume. Thus it is necessary to use ultrapure solvents and nanopure water for sample preparation. Residual fluorescence increases very rapidly with the energy of the exciting photon, and thus working in the blue or near-ultraviolet (UV) part of the spectrum will often give rise to more serious background problems. To illustrate the issues with Raman

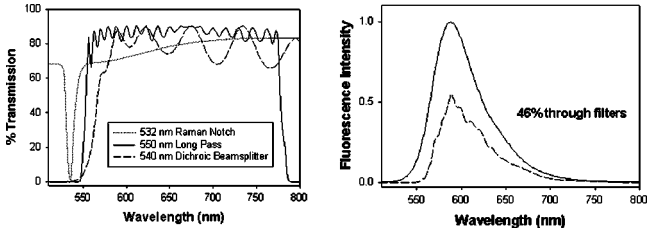

FIG. 2. Example of filtering considerations for SMS. The left panel shows transmission spectra of a 532 nm holographic Raman notch filter, a 550 nm long pass emission filter, and the transmission of the dichroic beamsplitter through which the fluorescence must pass. The right pane shows the emission spectrum of Nile red in methanol solution, and the resulting shape of the emission spectrum after passage through all three filters. The integrated area ratio shows that 46% of the fluorescence collected by the microscope objective passes through the filters.

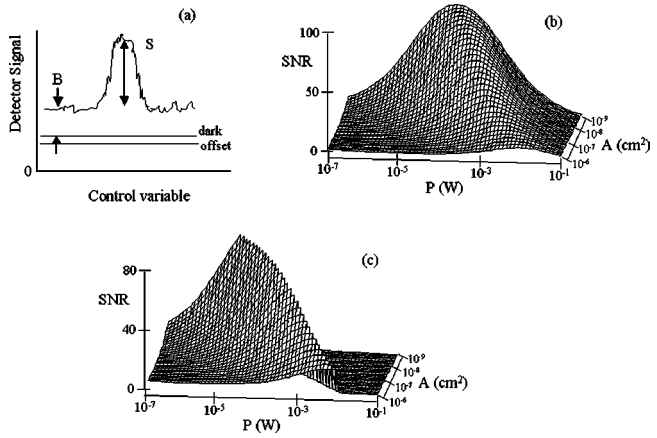

FIG. 3. SNR considerations: (a) for a hypothetical signal with control variable shown on the horizontal axis, the definitions of the offset, dark level, and background level B are shown. The signal from the single molecule is S. (b) Surface plot of fluorescence SNR vs probing laser power and focal spot area for a fluorophore with the following parameters: $\lambda = 532$ nm, $\tau = 0.1$ s, $\phi_F = 0.28$ (RG6 in water, Ref. 65), $I_S = 5.6 \times 10^3$ W/cm^2 (Ref. 69), $\sigma = 4 \times 10^{-16}$ cm^2, $D = 0.072$, $C_b = 2 \times 10^8$ counts/W s (measured in a typical confocal microscope), $N_d = 100$ counts/s. (c) SNR for the same model fluorophore assuming a photobleaching quantum yield of 10^{-5}.

scattering, one may consider benzene as a solvent. The total Raman scattering cross-section of benzene for one of its strongest modes is about 10^{-12} Å^2 (per molecule),[33] which gives a total cross section of less than 10^{-2} Å^2 for an excited volume of 1 μm^3. This shows that Raman scattering can become comparable to the absorption cross section of a single molecule in a solution at room temperature for excited volumes of about 100 μm^3. Given that the background cross sections are proportional to the excited volume, an optimal signal-to-background ratio will require a minimum excited volume, and all of the microscope configurations described in Sec. III work toward this goal.

As mentioned above, filters are generally required in order to suppress Rayleigh scattering of the pump radiation. To illustrate, suppose a single molecule of rhodamine 6G is probed with 1 kW/cm^2, somewhat below the onset of saturation of the absorption. The resulting incident photon flux at 532 nm of $\sim 3 \times 10^{21}$ photons/s cm^2 will produce about 1×10^6 excitations/s. With a fluorescence quantum yield of 0.9, about 9×10^5 emitted photons/s can be expected. At the same time, $\sim 3 \times 10^{13}$ pump photons/s illuminate a focal spot 1 μm in diameter. It is of course helpful in reducing the size of Rayleigh scattered pump radiation at the detector that photons are often collected in the backward direction. In any case, rejection of the Rayleigh scattered pumping radiation by a factor on the order of $10^7 - 10^8$ is generally required, with minimal attenuation of the fluorescence.

Thus, filtering for single-molecule experiments must attenuate Rayleigh scattering by the largest possible factor while transmitting the desired redshifted fluorescence from the single molecule. If additional suppression of host/matrix Raman scattering is desired, the transmission window of the filters can be further optimized to reject any strong (Stokes-shifted) Raman lines, but this must be done in a way that does not attenuate the precious fluorescence photons from the single molecule unduly. The required filtering for a specific experiment is generally accomplished by (in increasing order of performance) low-fluorescence glass filters (Schott), interference filters (Chroma, Omega) or by relatively expensive holographic notch attenuation filters (Kaiser). The filter characteristics must have a high slope in the filter transmission spectrum in order to open quickly enough as wavelength is increased to pass the single-molecule emission. Figure 2 illustrates the filter characteristics for a set of filters chosen for microscope experiments with the dye nile red pumped at 532 nm. The left side of the figure shows transmission spectra of: (a) a 532 nm holographic Raman notch filter, (b) a 550 nm long pass emission filter, and (c) a 540 nm dichroic beamsplitter through which the emitted fluorescence must pass (see microscope descriptions in Sec. III). The product of these three transmission spectra gives the wavelength dependent transmission factor F_{filter} that must be applied to the single-molecule fluorescence spectrum. Figure 2 (right side) shows the unperturbed nile red emission spectrum (upper trace), and the spectrum after passage through the three filters (lower trace). By comparing the areas of the two curves, $F_{\text{filter}} = 46\%$ of the nile red emission is passed on to the detector. The transmission at the pump wavelength is so small that it cannot be easily measured with a conventional UV-vis spectrometer, so direct measurement of pump laser transmission is preferrable.

C. SNR and signal to background ratio (SBR)

While many applications of fluorescence imaging have need of high signal-to-noise ratios, few are as demanding as single-molecule imaging at ambient temperatures. Now that the fundamentals of single molecule emission and the background issues have been described, the full set of factors that affect the SNR for single-molecule fluorescence experiments may be presented in a more quantitative fashion. Figure 3(a) illustrates the basic definitions of the various signal and background levels. In all experiments, there is a control variable (abscissa) that has the effect of making the single-molecule signal appear and disappear. For example, the control variable in a microscopic experiment would be spatial position defined either by the position of the focal volume or by the spatial position on the two-dimensional detector. (In the earlier low temperature experiments, the laser frequency

or the local applied electric field could also act as the control variable.) Starting from the zero level, some detectors have a constant dc offset value that is present even if there were no dark counts in the presence of no light. This offset is common in charge coupled device (CCD) detectors, and arises from the input offset of the sample and hold amplifier before the analog-to-digital converter. For all quantitative calculations, levels should be measured relative to this offset level. Above this offset level is the signal corresponding to the dark counts of the detector. The number of dark counts recorded should increase linearly with the counting time T, hence the proper value for the average dark count rate can be determined by recording without light for a range of T values. The background level B appears on top of the dark count level as shown in Fig. 3(a). If the source of background varies from spot to spot, then the average B level will not be the same at all values of the control variable. Finally, the single-molecule signal S appears on top of the sum of the background and dark levels.

The fundamental detection problem reduces to this: in order to observe the single-molecule signal S, the size of S must be compared to the fluctuations in S, B, and dark, because it is only when the fluctuations are large that the single-molecule signal is obscured. (That is, if the B and N levels were perfectly fixed, then they also would act like a simple offset that can be trivially subtracted from the data.) To express this quantitatively, Basché *et al.* have presented the following equation to compute the SNR for fluorescence detection of a single molecule,[74] based on the assumption that the noise factors limiting detection are the Poisson (shot) noise fluctuations of the single-molecule signal, the background signal, and the dark counts:

$$\mathrm{SNR}=\frac{D\phi_{\mathrm{F}}\left(\frac{\sigma_p}{A}\right)\left(\frac{P_0}{h\nu}\right)T}{\sqrt{\left(\frac{D\phi_{\mathrm{F}}\sigma_p P_0 T}{Ah\nu}\right)+C_b P_0 T+N_d T}}, \tag{10}$$

where ϕ_{F} is the fluorescence quantum yield of the fluorophore, σ_p is the absorption cross section, T the detector counting interval, A the beam area, $P_0/h\nu$ the number of incident photons per second, C_b the background count rate per watt of excitation power, and N_d the dark count rate. D is an instrument-dependent collection factor which is a product of the angular collection factor F_{coll} of the detection system [primarily dependent on the numerical aperture (NA)], the optical losses in optics expressed as a transmission factor F_{opt}, the filter transmission F_{filter} (see the previous section), and the detector quantum efficiency η_Q; $D=\eta_Q F_{\mathrm{coll}} F_{\mathrm{opt}} F_{\mathrm{filter}}$. For a detailed discussion of the F_{coll} factor for a single molecule taking into account the dipole radiation pattern, total internal reflection, and the molecular orientation, see Ref. 45. This factor depends upon the orientation of the molecular transition dipole moment relative to the propagation direction of the incident light. If precise detail of the collection is required, it is necessary to take into account the modifications of the dipole emission pattern that arise as a result of passage through dielectric interfaces of varying indices of refraction; molecular emission is more efficient into high-index media.[75] Typical values of D are in the range of 1%–8% for modern systems.

Assuming the collection efficiency D is maximized, Eq. (10) shows that there are several physical parameters that must be chosen carefully in order to maximize the SNR. First, as stated above, the values of ϕ_{F} and σ_p should be as large as possible, and the laser spot should be as small as possible. Higher powers produce higher SNR values, but the power P_0 cannot be increased arbitrarily because saturation causes the peak absorption cross section to drop from its low-power value as in Eq. (4). Various limits of Eq. (10) may be examined; for example, supposing that background $\gg$ dark counts, then the SNR at low power grows with the square root of power, peaks, and then eventually falls off when the saturated single-molecule signal becomes smaller than the background signal.

To illustrate graphically some of the tradeoffs inherent in Eq. (10), parameters for a model laser dye in the rhodamine family will be used to explore the SNR function in more detail. Assuming 0.1 s integration time and using a measured value of the background parameter C_b in a typical confocal experiment ($\sim 2\times 10^8$ photons/s W), Fig. 3(b) shows the computed SNR versus laser power and beam area. It is clear that for a fixed laser spot size, an optimal power exists which maximizes the tradeoff between the saturating fluorescence signal and the linearly (with P_0) increasing background signal. Following the surface plot at a fixed value of A, the SNR at first improves with increasing power, because the signal increases linearly with P_0 and the shot noise from the power-dependent terms in the denominator only grow as the square root of the laser power. As saturation sets in, however, the SNR falls because the signal no longer increases. Another relationship illustrated in Fig. 3(b) is that the best-case SNR at smaller and smaller beam areas levels off (the flattening of the ridge at small beam area). This is due to the effect of saturation and shot noise—at smaller and smaller areas the power must be reduced eventually to the point where the SNR is controlled by the shot noise of the detected signal [first term in the denominator of Eq. (10)].

It is important to emphasize that Fig. 3(b) illustrates the best case, in which the SNR is limited only by the Poisson fluctuations inherent in detecting photons. In practice, there are other effects that come into play which may act to reduce the attainable SNR in time T below the optimal values at the peak of the mountain in the figure. The most important limiting effect usually turns out to be photobleaching. Consider a given point on the surface plot defined by a laser power and a spot area, i.e., a particular value of laser intensity. If intensity is too high, then the molecule may not last long enough to provide photons throughout the counting interval T. Typical values of the photobleaching quantum yield ϕ_B are in the range 10^{-5}–10^{-7},[65,69] and the inverse of this parameter effectively determines the total number of emitted photons on average before photobleaching. To approximate the effect of photobleaching, Fig. 3(c) is a calculation identical to Fig. 3(b), except that when the number of emitted photons exceeds 10^5 (ϕ_B set at 10^{-5} for simplicity), the SNR is set to zero. The effect on the achievable SNR is

obvious, especially at the smallest spots and largest excitation power.

Faced with limitations due to photobleaching, the experimenter should make the power/time/SNR tradeoff carefully. By controlling the laser intensity, the rate at which photons are emitted can be easily varied up to the maximum rate. The experimenter can then choose which time scale is of the most interest: for fast time information, high laser intensities should be used to give the best possible SNR in short counting intervals T before photobleaching. If long-time information is needed, it is better to work with much lower intensities and lower emission rates. It is even useful in some experiments to pulse the probing laser at low duty cycle and observe the molecule only briefly with long intervening dark periods. This is a very useful strategy especially if the photobleaching process is nonlinear. In all cases, it is best to minimize both the dark counts and the background sources to obtain the maximum information about the molecule.

It is worth noting that Eq. (10) applies to both wide-field as well as scanning confocal detection systems. In the case of wide-field experiments, it is the diffraction-limited focal area that controls the A parameter and the power through this area which gives the P value for the purpose of determining SNR. In the near-field case, on the other hand, the local electric fields around the tip are modified compared to the case for focused Gaussian beams.[76] Moreover, the molecular dipole interacts with the local electric field directly via the dot product squared, and a more detailed analysis is required which takes into account the field distribution as well as any other quenching interaction between the tip and the molecule.

Another often-quoted measure of signal size is the SBR. This parameter, though useful, is not as fundamental as the SNR given above. For this reason, definitions of SBR vary; one definition (for negligible dark counts) is SBR=(signal of interest+background scattering)/(background scattering), and another is SBR=(signal of interest)/(background scattering). The SBR and SNR both depend upon a number of parameters of the system, including incident intensity, collection and detection efficiencies, quality of sample, etc., and the SNR in addition depends critically upon the detection bandwidth determined by the integration time T. The SBR is independent of averaging time and is really only a measure of the brightness of the molecule compared to the overall quality of the sample and the ability of the detection system to reduce background. On the other hand, the SNR in a fundamental way senses the ability to detect the single molecule compared to the noise fluctuations that are present which may masquerade as a single molecule. If the background and signal are both large and emission saturation is not occurring, the relative effect of Poisson noise is smaller, and it becomes easier to detect the presence of a single molecule in spite of large background. Typical values of SBR for experiments with good fluorophores are on the order of 3–10 or more.

D. Detectors for single-molecule experiments

As is evident from the above SNR discussion, detecting SM fluorescence requires a device that can detect single photon arrivals with minimal dark noise, and the ''photon budget'' imposed by irreversible photobleaching effects demands that the quantum efficiency be as high as possible for single-molecule fluorescence detection. There are essentially two classes of detectors for SMS experiments: single-element detectors and two-dimensional array detectors. The capabilities and characteristics of various examples of each class will be discussed, as proper detector selection is central to the success of SMS experiments.

1. Single-element detectors

Early experiments observing the flow of single dye molecules through a tightened laser focus detected photons with a high-quality microchannel plate photomultiplier tube (PMT),[77] since the PMT offered adequate temporal resolution to observe the short bursts of fluorescence as small dye molecules diffused through the laser focus. While PMTs offer suitable temporal response and can have quite low dark noise levels when cooled, they suffer from low quantum efficiencies for visible light ($<20\%$), limiting their use in SMS experiments. Further, PMTs require several pieces of low-noise electronics to efficiently detect single photons, and even with cooling, dark count rates in the 10–100 cps range are common. PMTs do have a large area of detection on the order of 1 cm$\times$1 cm, so this may be an advantage in some cases.

As an alternative, recent advances in semiconductor photodetectors have allowed for the commercial availability of avalanche photodiodes (APDs) capable of detecting single photons in an integrated package that contains on-board amplifiers and cooling, thus diminishing dark counts to levels as low as 25 dark counts/s. These units, called single photon avalanche photodiodes (SPADs) have much higher quantum efficiencies, $>60\%$ across the visible spectrum, even approaching 95% in the near-infrared (IR) as a result of the band structure of Si. The engineering of these detectors makes the SPAD much easier to use than a PMT; the module requires low operating voltages (5 V), generating the high voltage for biasing of the APD internally. A detected photon is converted to a digital (TTL) output pulse that can be easily counted on a computer-based digital acquisition board. Typical temporal response for the SPAD is comparable to PMTs; photons can be detected with an accuracy of $\sim$350 ps full width at half maximum (FWHM); however, the detector has a larger ''dead time'' between photon arrival events thus limiting the maximum count rate. Faster SPADs are available, but their increased temporal response generally comes at the expense of lower quantum efficiencies. In terms of dark counts, units are commercially available with 100 cps, 50 cps, even down to 25 cps, but the cost increases dramatically as the dark count rate goes down. The only disadvantage of the SPAD compared to the PMT for SMS experiments is that the SPAD detector has a much smaller active area (180 μm diameter). This limitation can easily be overcome in SMS confocal or near-field microscopy experiments, since the spot size at the microscope image plane can easily be made to underfill the SPAD detector chip. The small active area has even been used as a confocal aperture in confocal imaging applications. Because of its ease of use and superior quantum

efficiency the SPAD has become the standard single element detector for SMS. Further technical details of the SPAD are described in Ref. 78.

2. Two-dimensional array detectors

For wide-field microscopic applications, any one of several ultrasensitive cameras may be used for the detection of single-molecule fluorescence; indeed part of the reason that single-molecule studies have become widespread is the continuing advance in CCD detector array technology that has occurred over the last decade. Even the human eye, when properly dark adapted, can see the light from a single molecule in the eyepiece of a microscope that efficiently collects the emitted photons. The use of a commercial camera for amateur astronomy has also been used to observe single-molecule emission,[79] but such detectors are relatively slow to read out, sometimes taking minutes to transfer one frame to a computer. Here a selection of modern CCD array detectors is described.

Liquid-nitrogen cooled, back-illuminated Si CCD array detectors (Princeton Instruments) have been available for some time for applications in astronomy and spectroscopy. The back illumination provides quite high quantum efficiency in the red and infrared, up to $\sim 70\%-80\%$. Liquid-nitrogen cooling provides the cold sink for operation at a temperature near $-120\,^{\circ}\mathrm{C}$, and this temperature is carefully chosen to enable charge motion and drastically reduce dark counts, down to levels near 1 electron/pixel/h. Thus, this and other CCD detectors may be viewed as a collection of $256 \times 256 = 65{,}535$ high-performance photon counting devices! The major limitations of this type of detector are: (a) the low temperature limits the speed at which electrons can be read out, and (b) a penalty of 10–20 electrons of read noise is paid for each analog-to-digital conversion. Thus, these detectors are best for cases where long averaging times are acceptable, such as in recording the spectrum of the fluorescence from a single molecule.[80–84] In this situation, the counting interval is made long enough so that enough photoelectrons are collected to overcome the readout noise. Naturally, for long averaging times, the spikes that arise from cosmic rays must be removed from any images or spectra.

Intensified frame transfer Si CCD cameras, such as the I-Pentamax (Princeton Instruments, now Roper Scientific) have been commercially available since the early- and mid-90's. In this design, photons are first detected by a multialkali photocathode, and the electron emitted is amplified (''intensified'') in a microchannel plate coupled to the photocathode by a fiber bundle. The resulting group of electrons hits a phosphor screen to generate photons again, a front-illuminated Si CCD detector converts the phosphor photons into electrons, and the electrons from each CCD well are ultimately converted into a digital number using a fast analog-to-digital converter (ADC). The CCD and/or photocathode may be Peltier cooled to reduce noise from thermionic emission. The primary advantage of this design is the multiplication of the detected photoelectron before any read noise penalty is paid. This means that even one detected photon can be recorded, and the readout noise of the CCD becomes less important. As a result, a faster ADC (~ 5 MHz conversion rate, with a noisier buffer amplifier) can be used, and detectors in this class can run at video frame rates and higher. Continuous readout with very small dead time is enabled by the frame-transfer mode of operation, where only half of the CCD is illuminated; after a frame, the illuminated half is shifted into the hidden half, and readout of the hidden half commences during the next illumination time. Limitations of this detector arise from the somewhat lower quantum efficiency of the photocathode material, excess noise that may arise from the multiplication process, nonuniform gain over the various channels of the intensifier plate, and the danger of detector damage by excess light.

A sensitive back-illuminated, nonintensified frame-transfer CCD camera (Micromax, Roper Scientific) has been available for several years. This design capitalizes on improvements in design of back-illuminated chips so that faster ADCs can be used without large increases in readout noise. In a typical system, 5 MHz readout rate with 11 electrons/pixel read noise has been observed. Advantages of this design are the higher native quantum efficiency of Si, the much higher degree of uniformity in sensitivity from pixel to pixel, and the lack of intensifier-related distortions. Of course, without multiplication, the camera is better suited for brighter fluorophores, i.e., the read noise must be overcome to detect photoelectrons.

Very recently, frame-transfer Si CDD cameras with on-chip multiplication gain have become available (Cascade, Roper Scientific; iXon, Andor Technology). This design uses a CCD chip that operates for the most part like a standard CCD except that the last row of CCD wells is connected to a series of additional wells on the chip biased so as to have a small amount of secondary emission as the electrons are passed from well to well. The net effect is a multiplicative gain factor of up to $\sim 100\times$ on the chip, before any read penalty is paid. This detector may find widespread application since it combines the virtues of Si as a photodetector with relative insensitivity to readout noise. Moreover, the fully integrated design means that the optical configuration is much simpler than the intensified CCD in which a photocathode, fiber bundle, microchannel plate, phosphor, and CCD must all be optically cemented together.

Other specialized detectors can be used for single-molecule microscopy. One example is the resistive anode microchannel plate detector, which is effectively a large-area PMT in which the detected signal is located in $x-y$ position by a form of spatially dependent readout (e.g., Photek, Roentdek GMBH). This detector can provide fast timing information, at the expense of lower quantum efficiency and a limited maximum detection rate—each photoelectron must be swept out of the device before another arrives.

III. MICROSCOPE CONFIGURATIONS

Several optical configurations have been demonstrated to satisfy the basic requirements for single-molecule detection and spectroscopy, where the molecule is studied for an extended period long compared to the diffusion time through a focused laser spot. Successful microscopic techniques in-

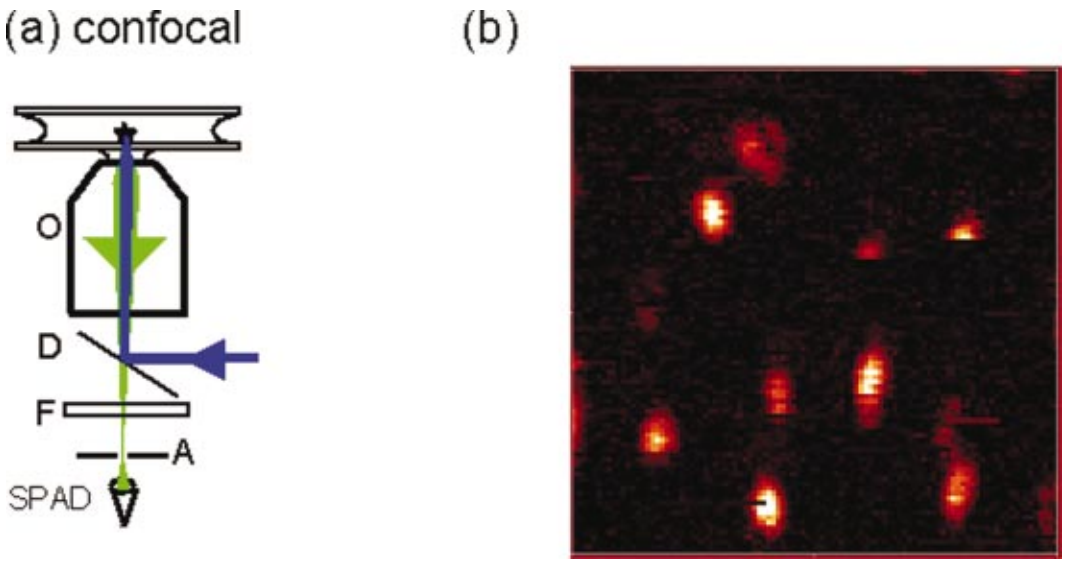

FIG. 4. (Color) Confocal microscopy. (a) Schematic of experimental setup (O) objective, (D) dichroic beamsplitter, (F) filters, (A) confocal aperture to restrict axial extent of the sample that can lead to scattering backgrounds, and (SPAD) silicon photon counting avalanche detector. (b) Example confocal image of nile red single molecules in a PMMA thin film. $\lambda = 532$ nm, laser intensity 1.1 kW/cm^2, 100 by 100 pixel image, 10 μm$\times$10 μm field at the sample plane, 10 ms dwell per pixel, total acquisition time 100 s. The fluorescence was filtered with a 540DRLP dichroic beamsplitter (Chroma), E550LP emission filter (Chroma), Raman Super Notch Plus 532 (Kaiser Optical) emission filter, imaged through a 75 μm confocal aperture, and detected with a SPCM-AQ-141 SPAD (EG&G). The point spread function of the microscope is slightly elongated in the vertical direction.

clude scanning methods such as near-field scanning optical microscopy (NSOM) and confocal microscopy and wide-field methods such as total internal reflection and epifluorescence microscopy.

A. Scanning methods

One family of SMS techniques involves illuminating the sample with the smallest spot possible and scanning either the illumination spot or the sample itself. An image is constructed point by point, and when an immobilized single molecule is located, it can be studied by positioning the laser spot directly over the molecule. While scanning methods lack the ability to observe several isolated single molecules in parallel, and thus prevent real-time observation of motion over microscopic distances, the smaller illumination volume used lowers background, improving the SNR. Additionally, the detectors used in scanning experiments offer higher temporal resolution than the CCD cameras used in wide-field experiments, whose temporal response is limited by the ability to read out the CCD detector array. Thus, for experiments that require maximum sensitivity and temporal resolution, scanning methods are the preferred SMS method. The two primary scanning methods used will be highlighted below: confocal microscopy, in which a diffraction-limited laser spot is the point source, and NSOM, where so-called ''near-field'' effects create a laser spot smaller than the diffraction limit.

1. Confocal microscopy

Figure 4(a) shows a simplified schematic of a confocal microscope. A collimated laser beam is reflected off of a dichroic beamsplitter and through an infinity-corrected, high NA microscope objective, with the result that the laser is focused to a diffraction-limited spot at the sample plane. The diameter of the laser focus can be defined by several criteria, such as the well-known Rayleigh criterion,[85] the Sparrow criterion, or others. The Sparrow criterion states that two points of equal brightness can be distinguished if the intensity at the midway point is equal to that at the points (i.e., the gradient at the peak of the summed profile is zero), and is given by: $d_s = 0.51\lambda/\mathrm{NA}$, where λ is the excitation wavelength. Thus, for $\lambda = 488$ nm a NA$=1.4$ (oil) objective will give $d_s = 178$ nm, while a top-quality air objective, NA $=0.9$ produces a spot with $d_s = 277$ nm. Since the background scattering scales with the illumination area, a high-NA objective helps the SNR by both increasing the signal (collecting more light) and by reducing background.

Emitted fluorescence and backscattered laser light are then recollected and recollimated by the same microscope objective and pass through the dichroic beamsplitter. Residual laser light is then filtered out as described above, and fluorescence is focused by the microscope tube lens through a pinhole aperture located at the microscope image plane. The pinhole serves to spatially reject out-of-focal-plane light, and gives improved axial resolution, known as the confocal advantage. The diameter of the pinhole determines the absolute depth of field for a confocal image, and an excellent treatment of pinhole selection is given elsewhere.[86] Note that the confocal advantage also helps with SMS, since a smaller depth of the matrix surrounding the single molecule is allowed to present photons to the detector, reducing background. This can be especially important in biological systems, where out-of-focus cell autofluorescence needs to be minimized.

Due to the limited number of photons available from a single-molecule emitter, selecting the proper sized pinhole is very important. Smaller pinholes give superior axial resolution at the expense of transmission through the pinhole, and are more difficult to align. The magnification of the micro-

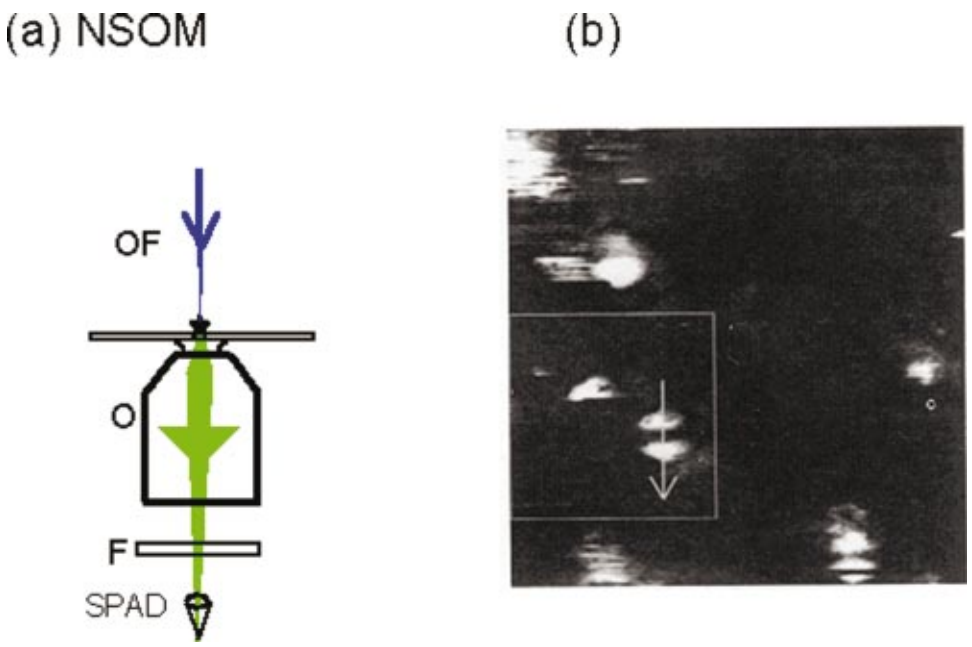

FIG. 5. (Color) Near-field scanning optical microscopy (NSOM or SNOM). (a) Schematic of a representative experimental setup: (OF) pulled and metal-coated optical fiber representing a near-field source of illumination that is placed very close to the sample surface, (*O*) objective, (*F*) filters, (SPAD) silicon photon counting avalanche detector. (b) NSOM image of single molecules of R6G on a silica surface using laser excitation at 514 nm. Field of view: 2.6 μm$\times$2.7 μm, peak signals represent $\sim$250 photocounts in 20 ms, and the gray scale signifies large signal (white) to low signal (black) (from Ref. 91, used by permission).

scope objective also influences the transmission through the confocal pinhole, since the size of the image spot at the pinhole is simply the diameter of the diffraction-limited laser spot multiplied by the objective magnification. For a 60$\times$ microscope objective, a 75 μm diameter pinhole allows high transmission ($>$90%), gives good axial resolution ($<$200 nm), and is easily aligned with a simple three-axis micrometer stage. Following the pinhole, the laser light is reimaged onto either a single element detector, such as the SPAD described above, or it can be dispersed by a monochromator onto a CCD to obtain single-molecule emission spectra, a technique that will be detailed below.

A confocal image is created by raster scanning the sample stage underneath the laser spot, typically with a computer-controlled piezo-electric stage. For confocal SMS, the resolution of the piezo stage should be better than 50 nm, and a closed-loop piezo scanner makes it much easier to locate and remain positioned directly on top of a single molecule, but is not absolutely necessary. A typical confocal image of single nile red molecules embedded in a thin poly(methylmethacrylate) (PMMA) file is shown in Fig. 4(b). The two-dimensional (2D) image is 100 by 100 pixels, representing a 10 μm$\times$10 μm area, and is acquired in 100 s. Each pixel has a 10 ms dwell time and the total number of photons counted in that time are displayed in a colorized gray scale, ranging from dark (fewer integrated photons) to light. The image was scanned horizontally from the top to bottom; several of the nile red molecules showed fluctuations during the scanning; and others showed photobleaching as evidenced by the spots that are cut off before the scan over the molecule is complete.

2. Near-field scanning optical microscopy

NSOM is another scanning method that is used for SMS. Figure 5(a) shows a simplified schematic for a near-field scanning microscope. Unlike the previously described ''far-field'' techniques, which are all governed by classical optics, near-field optics can be used to generate a laser spot smaller than the diffraction limit by using an aperture with a diameter much smaller than the wavelength of light and by detecting the light that leaks through this small hole. If the radiation that propagates through this small hole is detected in close proximity to this aperture, that is within an axial distance on the order of the aperture diameter (far below the optical wavelength), the spot size detected will be that of the sub-wavelength aperture. Of course, as the axial distance from this aperture increases, the spot size increases rapidly, reaching the diffraction limit in the far-field regime. The idea of near-field optics has been widely known for some time; it was first described by Synge in 1928 and initially demonstrated for microwave wavelengths in 1972 (see Ref. 87).

Near-field processes are characterized by low intensity throughput for light through these tiny apertures. In the early studies, to create a relatively efficient aperture suitable for optical wavelengths, a single-mode optical fiber was heated and pulled until it fractured, forming a tip much smaller than the original fiber core.[88] The fiber is then coated on the sides with thin film of a metal, such as Al, thus making a waveguide for the light with a tiny aperture at the end, which is typically 70 nm in diameter. Other improvements in near-field tips have recently appeared; for a review see Ref. 89. Using scanning technologies developed for probe techniques, such as atomic force microscopy, the fiber can be held at a distance $\sim$5 nm from the surface and scanned. Transmitted

light and fluorescence can then be collected in the far field by traditional optics, and the signal detected with a single element detector, as with a confocal microscope.

The first SMS experiments at room temperature were performed in 1993, using NSOM to image single $DiIC_{12}$ molecules embedded in a thin polymer (polymethylmethacrylate) film.[90] Strikingly, the authors observed varying fluorescence emission patterns that were indicative of the absolute orientation of the $DiIC_{12}$ molecules in the polymer film and analyzed them by considering the interaction with the inhomogeneous near-field electric field and the molecular transition dipole. NSOM has also been used to record fluorescence spectra of single molecules at room temperature, revealing heterogeneity among the spectral properties of single emitters as a function of time,[83] and has been used to measure single-molecule fluorescence lifetimes.[91–94]

The primary advantages of NSOM are: (a) the reduced sample volume that is offered by the reduced laser spot size, generating lower background counts, (b) immediate orientation information, and (c) the fact that monitoring the position of the scanned fiber tip gives topographic information simultaneously with fluorescence images. However, NSOM has several limitations, most notably that the pulled fiber tips are brittle and are subject to breakage, especially over samples with high surface roughness, limiting this technique to flat samples. It is also not possible to image single molecules far from the sample surface, since the near-field regime quickly disappears in the z direction, preventing the use of NSOM in many biological systems, such as in a cell interior. Further, even though many improvements have been made in probe design, the typical coupling efficiency through a pulled fiber is $\sim 10^{-5}-10^{-6}$ and it is difficult to consistently make fibers with the same aperture size. Finally, the modest increase of spatial resolution comes with greatly increased experimental complexity when compared to confocal microscopy. As a potential solution to some of these issues, novel apertureless NSOM techniques have been proposed, in which an ultrasharp tip is used as an antenna to localize the excitation region, and this technique may find further utility in single-molecule studies.[95–98] Another approach to ultraresolution involves stimulated emission depletion in the region encircling the focal spot,[99] but this method has not been applied to single molecules to date.

Figure 5(b) shows a typical NSOM image of R6G molecules on a cover slide over a 2.6 μm$\times$2.7 μm range.[91] The bright spots correspond to single chromophore fluorescence. The diameter of the spots is roughly indicative of the resolution of the microscope, demonstrating lateral resolution slightly beyond the diffraction limit, a tradeoff that was made in this particular experiment to obtain a higher count rate from the molecules. In the white boxed region, the two-lobed structure at the right is the ''image'' of a single molecule as expected due to polarization effects.[76] The left molecule in the box photobleached halfway through the time required to scan over the molecule. The arrow shows a subsequent and different scan direction that was used to collect fluorescence lifetime as a function of position, illustrating the strong alterations in excited state lifetime that occur due to interactions between the metal tip and the molecule.[91]

B. Wide-field methods

Perhaps the simplest method to observe single-molecule fluorescence is to use wide-field microscopy. As the name implies, a laser or arc lamp is used to illuminate an area several microns in diameter, as in a traditional microscope. Proper filtering is used to eliminate excitation light and to pass the single molecule fluorescence to a two-dimensional array detector, usually a CCD as described above, though the best single molecule emitters can even be observed with one's own properly dark-adapted eyes! (Not only can the molecules be seen with the unaided eye, the colors can be sensed, as well as color changes and amplitude fluctuations or blinking.) Performing SMS in this fashion has two major advantages: many individual chromophores can be observed simultaneously, and the position of chromophores can be monitored at near video rates, allowing researchers to observe translation of single molecules in real time. The primary limitation of wide-field microscopy methods is that the maximum frame acquisition rates for CCD cameras is slower than the response time for single element detectors, but for experiments requiring maximum temporal resolution on the order of 50 ms, wide-field methods have become a popular and useful SMS technique.

Even though a large region of the sample is imaged onto the detector image plane, the spatial resolution of wide-field techniques is diffraction-limited if research-quality microscope objectives are used. Thus, with high NA optics, single molecules will be imaged as spots on the CCD with $\sim$300 nm diameter (FWHM) referenced to the sample plane. However, it should be noted that with sufficient SNR it is possible to pinpoint the location of these spots to better than the diffraction limit. The accuracy with which the emitter's position can be determined is controlled by the size of the CCD pixels and the overall magnification of the microscope. Specifically, for a CCD camera with 15 μm$\times$15 μm pixels mounted on a microscope with a 100$\times$ objective and a 5$\times$ beam expander lens at the intermediate image plane (giving a 500$\times$ total microscope magnification), a wide-field image would display a single molecule as a spot that is 10 pixels in diameter, with a Gaussian intensity profile. The position of the center of this spot can easily be known to the nearest pixel, or 30 nm in this case, a concept that is key in studying diffusion or other similar processes. Again, with sufficient SNR, by fitting the illuminated pixels to a Gaussian profile, the center can be located to a position even small than the nearest pixel. In principle, infinite spatial resolution can be obtained (for one spot only; the limitations on the ability to resolve two spots still apply unless multiple colors are used to distinguish overlapping spots[100]) by dispersing the image over a greater number of CCD pixels, either by using a CCD with smaller pixels, a larger pixel array, or by increasing the magnification, but several factors prevent this. First, single-molecule photobleaching limits the total number of detected photons, and one needs to have a sufficient number of photons per pixel for a given integration time to maintain a proper SNR. Second, CCD cameras typically have read-out noise, which places limits on the degree to which the emitted photons can be spread over detector pixels. Finally, the read-

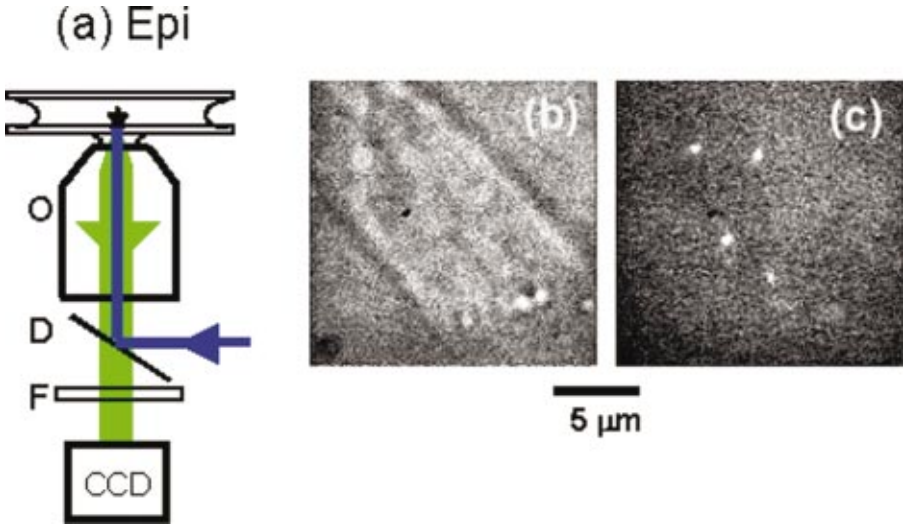

FIG. 6. (Color) Epifluorescence microscopy. (a) Schematic of a representative experimental setup: (*O*) objective, (*D*) dichroic beamsplitter, (*F*) filters, (CCD) two-dimensional array detector. (b) White light transmission image of a single CHO cell; various organelles in the cell interior are weakly visible. (c) Epifluorescence image for a 100 ms integration time of the same cell, showing the emission from single Cy5-labeled MHCII complexes as described in the text. Laser illumination at 633 nm provided an intensity of ~ 5 kW/cm^2 at the sample plane. The epifluorescence was collected with a 100× magnification, 1.3 NA, oil-immersion objective (CFI PlanFluor, Nikon, Burlingame, CA) and imaged through a 645 nm dichroic mirror and a 670 nm band-pass filter (Omega Optical Inc., Brattleboro, VT) on an intensified frame-transfer CCD camera (I-Pentamax, Roper Scientific, Trenton, NJ). The SBR was 1.6. The average SM signal without background was 751 ± 206 counts, and the average background was 477 ± 77 counts. (From Ref. 103, used by permission.)

out speed of a CCD camera roughly scales with the inverse of the number of pixels being read out per data acquisition frame, and one must carefully decide what parameters ensure the optimal balance of spatial and temporal resolution. Indeed, the parameters given above are typical for a modern intensified CCD camera and give adequate SNR for ''good'' single-molecule emitters, such as Rhodamine 6G (R6G), with 50 ms integration times.

There are two popular techniques for wide-field SMS imaging: epifluorescence and total internal reflection (TIR) microscopy. We will discuss the implementation of each technique and the relative advantages and disadvantages of each method below.

1. Epifluorescence

An epifluorescence SMS microscope can readily be constructed from commonly available commercial microscopes, as epifluorescence has been used for many years for biological applications in particular. This method was first applied to room-temperature SMS in studies of biomolecular motors.[101] Figure 6(a) shows a simplified diagram of an epifluorescence microscope for SMS. To illuminate an area several microns in diameter, it is necessary to use an input beam that is *not* collimated. A simple method to create a laser spot of appropriate diameter is to focus the laser beam onto the back aperture of the microscope objective. This is most easily accomplished using a lens with a focal length long enough that the lens can be mounted externally to the microscope; a typical lens used has a 0.5 m focal length. The input laser beam is then reflected toward the microscope objective by a dichroic beam splitter. The microscope objective should have the highest magnification available for most wide field applications for the reasons discussed above. For all SMS experiments, the NA is also a key parameter. NA $= n^* \sin \phi_{\max}$, where n is the refractive index of the medium between the sample and the objective and $\phi_{\max}$ is the maximum collection angle of the objective. To maximize the detected light, the NA should be as high as possible, and this is usually accomplished by using an objective designed to be immersed in a high-n medium. For most SMS applications, an oil immersion ($n = 1.51$) objective is preferred, and these objectives have an NA as high as 1.4. For imaging in some biological environments, it may be favorable to implement a water immersion ($n = 1.33$) objective, which usually has NA = 1.2, exchanging some light gathering ability for improved image quality, but for most SMS experiments, the oil objective is preferable. Naturally, the oil used must not contain fluorescent impurities. The flatness of field for the microscope objective also has a significant bearing on wide-field imaging applications, especially if distance parameters across the image need to be carefully quantified. Microscope objectives designated ''PlanApo'' are designed with the highest flatness of field and color correction, and should be used for all wide-field imaging. For imaging at short wavelengths, it also may be necessary to choose a microscope objective with very low fluorescence.

Fluorescence emission is collected back through the same microscope objective and transmitted through the dichroic beam splitter. Residual laser excitation light is rejected by appropriate long pass filters and/or notch filters, as highlighted earlier. The light is then focused via the microscope tube lens to a CCD camera. If additional magnification is desired, relay lens systems with magnifications $2\times - 8\times$ are commercially available and are easily installed into the microscope.

One of the applications of wide-field SMS is the study of motion of critical structures in the membrane of single cells.[102] Single-molecule labels are preferred to multiple labels or large beads in order to minimize disruption of native structures. One recent effort has explored diffusion of single

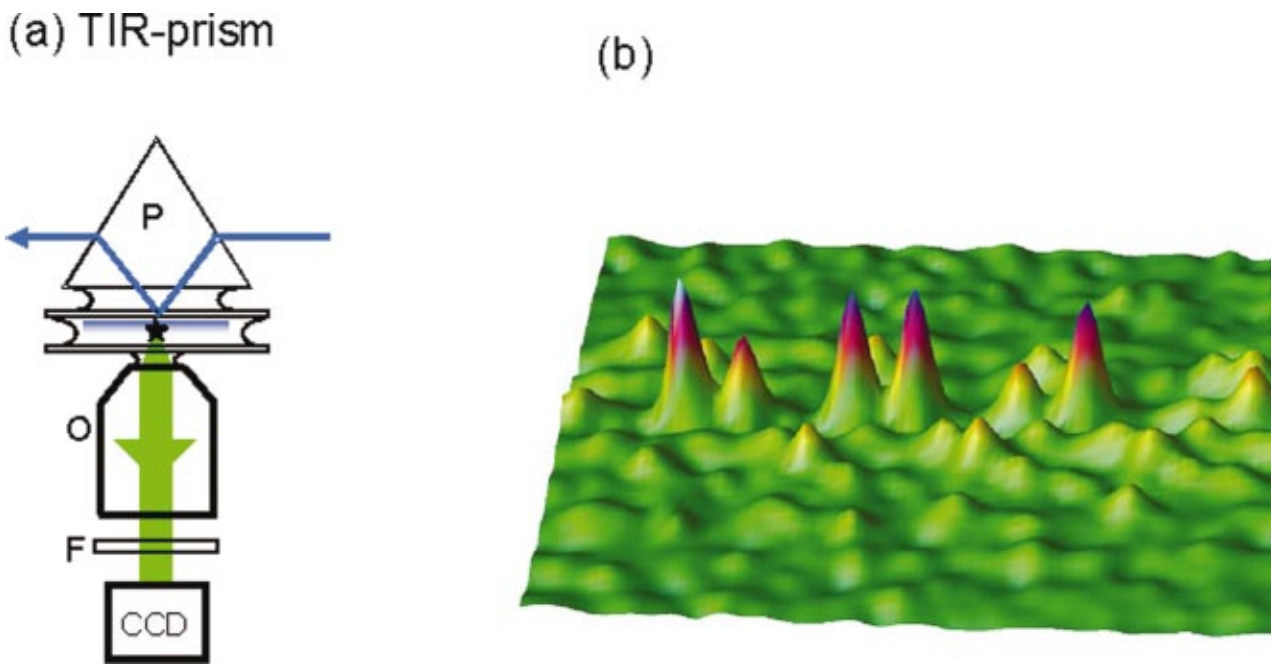

FIG. 7. (Color) Total internal reflection microscopy using a prism. (a) Schematic of a representative experimental setup: (P) prism, (O) objective, (F) filters, (CCD) two-dimensional array detector, with the emitting single molecule signified by a star. (b) Image of the fluorescence emission over a 2.4 μm $\times$2.4 μm region from single copies of the GFP mutant T203Y immobilized in PAA in the TIR microscope. Conditions: pH 7, 100 ms exposure, and 2 kW/cm^2 of 488 nm pumping light at the gel-cover slip interface. Fluorescence was imaged with a Nikon Diaphot 200 inverted microsccope, 100$\times$ 1.4 NA PlanApo oil-immersion objective, via a 515EFLP long-pass or 535DF55 band-pass filter (Omega Optical) on a frame-transfer, intensified CCD camera (Princeton Instruments I-Pentamax) (from Ref. 109, used by permission).

transmembrane proteins embedded in live cells.[103] Briefly, diffusion of the Major Histocompatibility Complex of Type II (MHCII), an essential binding protein for T-cell recognition, was studied to determine how these important proteins move around in the cell membrane. Chinese hamster ovary (CHO) cells were selected because they adhere nicely to glass microscope coverslips and because the surface opposite the adhered side is extremely flat. Figure 6(b) shows an image of a CHO cell under white light illumination. The edges of the oblong cell are clearly seen in this image. To label the MHCII proteins in an unintrusive manner, a short polypeptide that strongly binds to the MHCII is labeled with a single Cy5 dye molecule and the cell is exposed to these proteins, which then bind to the MHCII structure in the cell membrane. Figure 6(c) shows an epifluorescence image of the labeled cell. Only dye labels at the surface away from the glass are visible because the depth of field in an epifluorescence microscope is $\sim$300–500 nm and the CHO cell is several microns thick. The authors were able to monitor the diffusion of the MHCII proteins by tracking the positions of the Cy5 labels with 100 ms integration times.

2. Total internal reflection

TIR microscopy can also be used to observe single molecules with high sensitivity. TIR measurements make use of the exponential decay of the evanescent field generated upon total internal reflection at a high-index to low-index boundary, most typically at the interface between a glass or quartz coverslip and air or water. For angles of incidence measured from the interface normal (θ) above the critical angle, the evanescent field intensity (I), (which is proportional to the square of the electric field amplitude), drops off with distance z into the low-index medium according to

$$I(z) = I(0)\exp(-z/d), \tag{11}$$

where $I(0)$ is the intensity at the interface, and the exponential decay distance d is

$$d = \frac{\lambda_0}{2\pi}(n_2^2 \sin^2\theta - n_1^2)^{-1/2}, \tag{12}$$

where λ_0 is the wavelength of the excitation light in vacuum, and n_2, n_1 are the indices of refraction of the glass/quartz and the air/liquid, respectively. The angle-dependent decay constant d is typically $\sim$150 nm for green laser excitation, and the small size of this parameter shows that the pumping excitation extends only a short distance into the low-index medium. Hence, the primary asset of TIR-based microscopy is that only fluorophores that are sufficiently close to the coverglass–air/water interface will be excited, while those further out in the bulk will not, and the volume of sample which can produce an interfering background is minimized. While TIR microscopy has been used for biological samples for a long time,[104,105] only recently has the method been applied to single-molecule studies.[101,106]

A TIR microscope can be implemented by coupling a microscope coverslip to a prism with an index matching fluid ($n = 1.51$ for glass). A laser beam can easily be coupled into the prism above the critical angle to achieve TIR, and the microscope can image the fluorescence excited from the evanescent field created at the interface. Figure 7(a) shows a schematic drawing of a prism-type TIR setup used to image single dyes[106] and single copies of GFPs embedded in a

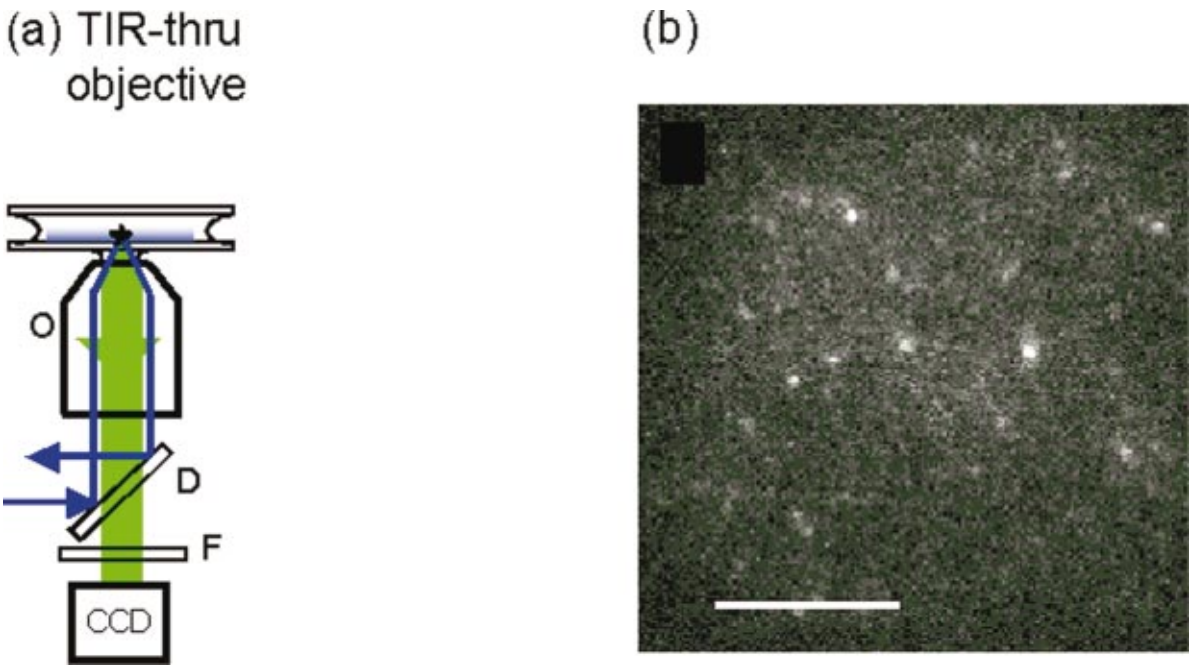

FIG. 8. (Color) Total internal reflection microscopy, through-the-objective configuration. (a) Schematic of a representative experimental setup: (*O*) objective, (*D*) dichroic beamsplitter, (*F*) filters, (CCD) two-dimensional array detector. (b) Example image of R6G in PMMA, scale bar 10 μm, incident intensity at 532 nm$=0.56$ kW/cm^2. This image was recorded with a TE300 inverted microscope (Nikon) with a 60×, 1.4 NA oil-immersion objective, 545LP dichroic filter, HQ525/50 emission filter (Chroma, Brattleboro, VT), and a frame-transfer, intensified CCD camera with 100 ms integration time (Princeton Instruments I-Pentamax) (from Ref. 110, used by permission).

water-filled poly(acrylamide) (PAA) gel matrix to restrict Brownian diffusion;[107] see Refs. 108 and 109 for more sample preparation information. For this experiment, illumination was provided by the evanescent wave generated by TIR of a linearly polarized laser beam at the interface between the quartz cover slip and the gel sample. The correct incidence angle for TIR on this interface was obtained by the use of a triangular quartz prism and a layer of glycerol on top of the upper cover slip. A quartz prism was used instead of glass to minimize background autofluorescence. Typical excitation intensities were of the order of 1 kW/cm^2, but of course, the distance of the molecules from the interface was not controlled, so the absolute intensity at each molecule could vary by as much as a factor of 2 or more. In typical measurements, saturation of the emission was avoided. Figure 7(b) shows a rendered three-dimensional plot of GFP fluorescence as a function of two-dimensional position in the microscope plane; it should be noted that this type of plot is yet another method to display single-molecule fluorescence image data, and it is easy to compare the relative intensities of individual molecules by examining relative peak heights.

TIR can also be created by coupling an input laser beam through the extreme edge of a high-NA microscope objective, in order to place the evanescent field at the position of the first boundary between a glass cover slip and a lower-index medium. The method is then called through-the-objective TIR, a technique first implemented for SMS by Funatsu *et al.*[101] Figure 8(a) shows the through-the-objective TIR microscope. As with the epifluorescence microscope, the input laser beam is not collimated, and identical optics can be used for both setups, by simply mounting the final mirror of the laser input path on a translation stage. The microscope can be switched between epifluorescence and TIR by simply translating this mirror such that the input beam is coupled through the edge of the microscope objective or through the center as described in detail in Ref. 110. Figure 8(b) shows an image of single R6G molecules embedded in a PMMA film.

The primary benefit of TIR is the reduced background that comes from the reduced illuminated sample thickness and the lower absolute powers that are required to illuminate the samples. However, TIR is usually limited in its use to regions located within $\sim$150 nm of the glass microscope coverslip, and for imaging away from the glass coverslip interface, such as the MHCII diffusion study described above, epifluorescence can be useful. In one report, TIR at the interface between the cell and the surrounding aqueous medium has been described.[111] Several detailed comparisons of the various TIR configurations have been presented.[110,112]

IV. SPECIFIC DETECTION MODALITIES

Since the inception of SMS over 10 yr ago, great efforts have been made to extract the maximum information from every photon emitted from a single fluorophore, often a difficult task due to the intrinsically small signals inherent in single-molecule fluorescence. The ability to observe individual members of an ensemble population has demonstrated that significant heterogeneity exists even among molecules in crystals. SMS has shown that molecules are very sensitive to their local environment, and this sensitivity can be exploited to gain new insights into a variety of processes. Numerous techniques have been developed that can characterize several physical properties, such as molecular orientations, macro-

molecular conformational changes, energy transfer processes, and even providing insight into the physics of fluorescence itself. The overriding theme is to obtain as much information from the emitted photons as possible by recording their polarization, time of arrival, wavelength, action spectrum, etc. To study diffusion effects, the position of the molecule is recorded as a function of time and the data are analyzed for departures from Brownian motion.[102,103,113] This section briefly introduces several useful SMS detection modalities, describes the general implementation of the concept, highlights a few recent achievements using each respective technique, and directs the interested reader to detailed articles available in the literature.

A. Polarization microscopy

Despite the fact that the spatial resolution of (diffraction-limited) optical methods is on the order of a few hundred nanometers, the extreme sensitivity of SMS to changes in local orientation allows one to probe effects on the molecular scale. One of the most powerful SMS techniques currently employed is polarization microscopy, which allows one to determine the exact angular orientation of single molecules. In most cases, the absorption and emission dipoles of highly fluorescent molecules are parallel, and this is assumed here for simplicity. One way to extract orientational information is via modulation of the excitation polarization [polarization modulation, (PM)]. The physical basis for PM is simple; the excitation of a molecular transition is dependent on the angular alignment of the excitation electric field vector $\mathbf{E}$ (polarization) and the molecular transition dipole $\boldsymbol{\mu}$, specifically the probability of excitation depends upon $|\boldsymbol{\mu}\cdot\mathbf{E}|^2$. For a single molecule, there is only a single transition dipole to consider, so there is a discrete polarization anisotropy of the fluorescence. If the molecule is static or rotating slowly with respect to the integration time, then one can observe a $\cos^2$ dependence of the fluorescence signal as the polarization of the excitation laser beam is rotated with respect to $\boldsymbol{\mu}$. Similar arguments apply to the emission polarization: because the molecular emission has the shape of the dipole emission pattern, detection of the emission in two orthogonal polarization channels allows extraction of information about the molecular orientation. For reviews of polarization microscopy of single molecules, see Refs. 114 and 115.

Excitation polarization modulation can easily be incorporated into a confocal or wide-field microscope by using an electro-optic modulator to rotate the polarization of a linearly polarized input laser beam.[116] Confocal PM geometries have been used to measure reorientations of dye molecules in polymer films[117] and hindered rotation of dye molecules linked to tethered DNA molecules in an aqueous environment.[118] Wide-field PM experiments have been used to observe molecular machines in real time, including the rotation of F1-ATPase,[119] and to study the rotational flexibility of single kinesin motor proteins as a function of nucleotide state, revealing a previously unseen highly mobile form when adenosine diphosphate (ADP) is bound, providing new insight into the complex walking mechanism for this important protein.[120,121]

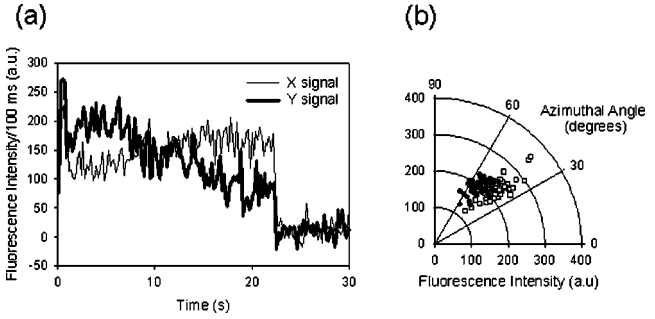

FIG. 9. Example of the use of polarization modulation microscopy to sense the in-plane orientation of the transition dipole moment of a single fluorophore on a single polymer chain. (a) Fluorescence emission with x and y polarized pumping as a function of time, illustrating a continuously changing in-plane dipole angle. (b) The trajectory of the in-plane dipole angle and the overall brightness of the molecule shown in (a), which shows the range of angles sampled by the dipole. The open squares and filled circles correspond to the early half and last half of the trajectory, respectively (from Ref. 50, used by permission).

As an illustration of the use of PM to extract orientation information for a single molecule in an epifluorescence experiment, Fig. 9 shows results for a singly labeled poly(butadiene) chain in a PMMA matrix.[50] The pump polarization was electro-optically toggled between two orthogonal transverse directions in the sample plane, denoted X and Y. The emitted fluorescence was collected through appropriate filters as usual, but with no analysis of the polarization. For each pump polarization, a 100 ms image of the single molecules was obtained. After the end of the experiment, the time trajectory of each of the molecules in the field was extracted, and data from a typical molecule is shown in Fig. 9(a). The ratio between the two emission signals clearly changes as a result of rotation of the molecule, up until the point of photobleaching at ~ 22 s. Figure 9(b) shows one way to display the data as a polar plot of in-plane angle with the radial position showing the total intensity of the molecule estimated using $(X^2+Y^2)^{(1/2)}$. From molecule to molecule, the dynamical character of such traces can change dramatically as a result of the hidden heterogeneity in an amorphous material.

An alternate approach to extracting polarization information involves pumping with circularly polarized light and resolving the emission into two orthogonal directions A and B.[122] In this case, the fluorescence polarization is usually calculated using $(I_A-I_B)/(I_A+I_B)$. If the molecules are rotating rapidly, the emission will be unpolarized and the detected P values will cluster around zero. However, if the rotation is slow, characteristic departures from $P=0$ will be observed. Some investigators have done both: PM as well as resolution of the emission, which can extract additional information such as the cone angle of a covalently attached fluorophore.[115]

It should be noted that TIR and NSOM geometries can introduce complicated polarization effects that can be used to further probe molecular orientations. In the case of TIR, p-polarized input laser light produces evanescent polarization in both the transverse and axial (z) directions, the latter of which can be used to excite molecular dipoles oriented in the z-axis direction perpendicular to the plane of the sample.

A prism TIR geometry was used to image the emission dipole orientation for single molecules by observing the emission patterns for single molecules,[123] capitalizing on spherical aberrations present when imaging several microns away from the glass cover slip with high-NA microscope objectives. This effect caused the z-oriented molecules to appear slightly defocused, giving them a ''doughnut'' emission pattern, whereas molecules with the transition dipoles aligned in the $x-y$ plane had a normal emission pattern. The local electric fields vary wildly across the aperture of an NSOM fiber probe, due to near-field effects described elsewhere.[76] Because the aperture is orders of magnitude larger than a single molecule, a molecule interacts with different local electric fields as the fiber is scanned across the molecule. The detected fluorescence intensity maps how the molecule interacts with these complex fields, and this can be used to probe the orientation of molecules, an effect originally seen in the first NSOM SMS experiments.[76] Other methods that have been to extract orientation involve annular illumination[124] and simultaneous resolution of the emission into three polarization directions.[125]

B. Spectral dispersion of emission

The previously mentioned single-molecule detection methods involve counting the total numbers of photons on a broad-band detector, usually a CCD camera or a SPAD, measuring total redshifted fluorescence as a function of time. It is also possible to obtain spectral information about single-molecule emitters as a function of time by using a modified version of the scanning SMS microscopes described above. Specifically, the single element detector can be replaced with a grating spectrometer to spectrally disperse fluorescence followed by a CCD camera placed at the slit position of the grating spectrometer. Each vertical strip of pixels on the CCD chip can be summed to create a ''superpixel'' that represents a single wavelength, and a complete fluorescence spectrum is then obtained with each frame read out on the CCD. One needs to realize that the emission spectrum from a single molecule has a SNR that is inherently worse than a wavelength-integrated signal, since the same number of photons is now being dispersed over many superpixels, which behave like individual detectors. Further, dispersion optics introduce additional optical losses in the microscope system. For this reason, high resolution grating spectrometers are seldom used in favor of low f-number systems with higher throughput.

The original single-molecule emission spectra were obtained for molecules embedded in solids at cryogenic temperatures,[80,81] a topic covered in several reviews.[82,126] Such spectra are actually equivalent to resonance Raman spectra, and the line positions show the Raman active modes of the electronic ground state. The primary benefit of working at low temperatures is that linewidths are extremely narrow, and it is easy to see small changes in the position of these sharp peaks. Further, even very weak lines are easily detected in the single-molecule spectrum since the photons for a given spectral feature are concentrated on a small number of pixels. Spectra have been obtained for single molecules embedded in a variety of crystalline[127] and polymer[80,81] hosts, revealing quite distinct spectral line positions arising from different local environments.

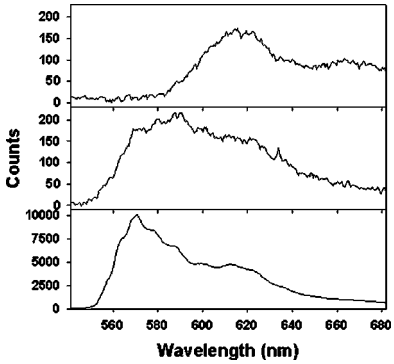

FIG. 10. A fluorescence spectrum of a single $DiIC_{12}$ molecule embedded in a PMMA film, recorded with the filtering described in Fig. 4, but obtained by directing the emission through a grating spectrometer to which a liquid nitrogen cooled CCD array detector has been attached. The excitation intensity was 1.5 kW/cm^2 at 532 nm. (Top and middle panels) Two different single molecules, with an integration time of 30 s. (Lower panel) Bulk spectrum, 1 s integration time, greatly attenuated laser intensity.

Emission spectra have also been acquired for single molecules at room temperature, revealing similar effects to the low temperature studies, including spectral diffusion and heterogeneity among the peak fluorescence positions for different molecules[83,84,92] and for extended chromophores in single polymer chains.[128] The primary difficulty in obtaining room temperature spectra is that linewidths are quite broad, typically on the order of 75 nm (FWHM) or more, making it challenging to trade off SNR and spectral resolution. A recent study[129] observed detailed variations in the local characteristics of thin polymer films by recording spectra from single nile red molecules, a polarity-sensitive dye able to sense charge transfer with the surrounding medium. The authors took spectra of nile red in relatively nonpolar PMMA and polar poly(vinyl alcohol) (PVA) films, measuring the position and widths of the fluorescence spectra. Interestingly, two distinct peak widths were observed for molecules in PMMA films, an effect the authors attribute to the presence of two domains in the polymer film with different local rigidities. Conversely, the PVA films showed a broad distribution of environments whose rigidity strongly depended on the level of hydration.

An example of fluorescence emission spectra from single molecules at room temperature is shown in Fig. 10. Single $DiIC_{18}$ molecules embedded in a PMMA film were illuminated with 1.5 kW/cm^2 532 nm laser light in a confocal microscope configuration. The top and middle panels show spectra from two different single molecules, with an integration time of 30 s. One may note how the individual molecules display radically different spectra, a result of different local interactions. For comparison, the lower panel of Fig. 10 shows a bulk spectrum taken with a 1 s integration time and greatly attenuated laser intensity for a film of many thousands of $DiIC_{18}$ molecules in PMMA. The ripples in the bulk spectrum are a result of the transmission characteristics of the microscope filters (see Fig. 2).

C. Fluorescence resonant energy transfer (FRET)

Another often-used fluorescence technique is FRET, where a short-wavelength ''donor'' fluorophore is pumped by a light source, and its energy is transferred to a longer wavelength ''acceptor'' molecule via Förster dipole-dipole interactions, whereupon the acceptor fluoresces, emitting light at a long wavelength. The FRET efficiency, E_d, is dependent on the distance between the donor and acceptor, and can be expressed: $E_d = 1/\{1+(R/R_0)^6\}$, where R is the distance between the donor and acceptor molecules, and R_0 is the characteristic distance where 50% of the energy is transferred from the donor to the acceptor. Under appropriate conditions, the energy transfer efficiency may be extracted from the ratio of the emission intensity of the donor to the emission intensity of the acceptor. Molecular factors that influence R_0 are the spectral overlap of the donor–acceptor pair, the refractive index of the medium, the quantum yields of the donor and acceptor, and the relative orientation of the transition dipoles for the donor and acceptor; typical R_0 values range from 2 to 6 nm. Excellent treatments of FRET are available in several monographs and reviews,[130–132] and single-molecule FRET has been the topic of a recent review.[133]

As a result of the sixth power dependence of E_d on the donor–acceptor distance, FRET is widely used to measure small distances between sites on large molecules such as proteins, and has been a useful bulk fluorescence assay for quite some time.[134] The spatial scale of FRET is far below the diffraction limit, so it is in principle possible to extract high resolution distance information in this manner. Recently, FRET has shown to be a powerful tool for using SMS to study conformational changes of biological macromolecules. Ha *et al.*[135] were the first to use FRET to detect conformational changes of a three-helix ribonucleic acid (RNA) junction, whose structure folds upon binding of the ribosomal protein S15. In this experiment, the authors used a confocal microscope, but split the detected light to two SPAD detectors using a dichroic beam splitter; the transmitted red (acceptor) intensity and the reflected blue (donor) intensity could then be monitored simultaneously.

One issue that should be considered with FRET on single molecules is the fact that the degree of energy transfer is extremely sensitive to the fluorescence properties of each dye molecule. Fluorescence dynamics can be extremely complicated for even the simplest systems, as shown above for the spectral diffusion of single molecules. Fluctuations in the fluorescence properties of the dyes themselves due to varying interactions between the dye and its local environment can drastically change parameters such as the emission spectrum and quantum yield, and these two properties may have to be measured separately in control experiments. Further, the rotational characteristics of the dye labels affect the orientational factor in R_0, and these can dynamically change on the time scale of the desired experiment. Since (for a fixed distance R) the FRET efficiency goes from a maximum when the donor and acceptor transition dipoles are aligned parallel to zero when the dipoles are perpendicular, one could mistake a conformational change for a rotational event if the relative dye rotation is slow enough. While these concerns are less of an issue with bulk measurements since the ensemble is a statistical average of all orientations, quantum yields, and other relevant fluorescence characteristics, one needs to perform many controls with a single-molecule system. Even small changes in the R_0 value will have huge changes in the FRET efficiency. For example, the rotational correlation times of the two dyes may need to be separately measured with polarization anisotropy to extract precise information.

Another limitation of FRET is that two separate dye molecules must be introduced to the system. Because the primary benefit of SMS is its inherent sensitivity to system heterogeneity, the two dye labels must be carefully introduced to the identical location of all studied molecules, and for proteins, the specific introduction of multiple dye labels is a challenging problem,[136] especially for those located inside living cells. However, fusions to GFP avoid this difficulty because the DNA that codes the protein for study can be genetically modified to include the DNA for GFP at a specific location in the DNA sequence, thereby creating a naturally fluorescent label at a known location. A recent effort in the Moerner lab[137] used a so-called ''cameleon'' construct that is a fusion of two GFP mutants to the Ca^{2+}-dependent calmodulin protein.[138] Upon binding Ca^{2+}, the cameleon protein contracts, pulling its two ends closer together. On one end of the cameleon, a blue-shifted variant GFP is expressed, and on the opposing end a redshifted GFP mutant is expressed. The authors pumped the blue donor GFP and were able to detect a significant increase in FRET efficiency (to the red acceptor GFP) upon Ca^{2+} binding, the first example of a single-molecule FRET system without using dye labels. However, the poor photostability of GFP reduced the amount of information obtainable.

In spite of these issues, single-molecule FRET continues to be a useful tool to study biomolecular dynamics. To address the orientational factor, often the two fluorophores are attached with floppy saturated alkane linkers to reduce the rotational correlation time. In addition, rather than attempting to extract precise values of the interdye distance R, large and qualitative changes in FRET efficiency are sufficient to conclude that the conformation of the system has changed. In addition to the studies mentioned above, single-molecule FRET has been used to study enzyme conformational dynamics,[139] the folding of individual RNA enzymes,[140] single GCN4 proteins,[141] DNA unwinding by Rep helicase,[142] and the list of experiments continues to grow.

D. Two-photon excitation

Recently, two-photon excitation of fluorescence has become a powerful tool for imaging biological systems in three dimensions, due to the quadratic dependence of two-photon excitation probability on laser intensity, a process that creates a vastly reduced excitation volume.[143] This aspect of two-photon microscopy can be thought of as an enhancement of the confocal advantage, where the depth of field is extremely thin, since the laser intensity outside the beam waist is much lower than that at the laser focus, allowing for superior cross-

sectioning ability. Indeed, the construction of a two-photon microscope is very similar to a confocal microscope using a femtosecond pulsed laser excitation source, except that the confocal pinhole is removed, since it is no longer needed. The primary advantages of two-photon microscopy are twofold. First, the reduced sample volume excites fewer background impurities, lowering background fluorescence. Second, it is possible to access transitions in the near UV using near infrared (IR) light, a powerful benefit since many materials fluoresce strongly when pumped in the near UV but are transparent to IR light, including cells and even the glass used in optical elements.

Two-photon single-molecule fluorescence was first reported in 1995 for single Rhodamine B molecules diffusing through the reduced two-photon laser focus.[144] Immobilized single molecules have also been observed with a comparable SBR to conventional confocal microscopy, but the probability of photobleaching was increased by approximately a factor of 2, possibly due to absorption of a photon while the molecule is in a dark triplet state,[145] a possible limitation inherent to this technique. There is also the possibility of heating of the host matrix or liquid by overtone absorptions. One must also take great care when focusing femtosecond pulsed light in a two-photon microscope; even modest powers can generate white light in the sample, limiting the intensity regime accessible to SMS experiments, which often require relatively high excitation rates to obtain an adequate SNR. Nonetheless, with the recent commercial availability of femtosecond pulsed lasers, the use of two-photon microscopy will continue to grow, especially for use in cellular systems and other thick samples that are subject to autofluorescence.

E. Time-dependent dynamical studies

No matter which experimental variable is measured, the time-dependent changes in the signal are usually of great interest. In fact, it is a particularly important advantage of single-molecule optical spectroscopy that the system under study can often be followed noninvasively as it proceeds through different time-dependent states. This dynamical information is an example of the type of information that is not easily available from ensemble averaged-measurements such as x-ray crystal structures or cryo-electron microscopy, for example. To be more specific, if a bulk ensemble sample is composed of enzymes in different chemical states, the states are often not synchronized and details of the state changes can be smeared out. However, a single-molecule experiment that follows the time-dependent behavior of each single molecule, one at a time, can remove this dynamic heterogeneity, without synchronization.

Time-dependent effects can arise on many different time scales, from nanoseconds to thousands of seconds, and they may arise from a variety of factors. Here the time scales of physical effects will be described proceeding from the fastest to the slowest, and examples of the type of analysis in each regime will be briefly mentioned.

1. Fluorescence lifetime measurements

On the shortest time scale of nanoseconds, the stream of photons emitted by the molecule contains information about the system encoded in the arrival times of the individual photons. One way to obtain information in this regime involves pumping the sample with short pulses from a repetitively pulsed source such as a mode-locked laser or a pulsed light emitting diode. After each excitation pulse, at most only one photon can be emitted since only one molecule is pumped. For sufficiently short excitation pulses, measurement of the distribution of time delays between the pump photon and the emitted photon allows a direct measurement of the excited state lifetime of the molecule τ_F. Once a single molecule is microscopically selected by any of the optical configurations shown above, the lifetime can be measured by the standard technique of time-correlated single-photon counting. In this method, digital timing electronics are used to measure the histogram of time delays for a set of pump photon–emitted photon pairs. For example, a specialized personal computer board (TimeHarp, Picoquant) can be driven by pulses signifying the time of the pump pulse and the time of detection of an emitted photon. Typically, the number of photons that must be detected to allow determination of the excited state lifetime is on the order of 100, with more photons required if high accuracy is needed. In actual experiments, the time resolution of the measurement is limited in the usual way by the instrument response function, and the maximum repetition rate is limited by the dead time of the detector. For the latter parameter, the SPAD detectors typically have larger dead times than PMTs, but there are other advantages of the SPAD detectors as described above.

The earliest single-molecule lifetime measurement involved flowing stream studies,[146] followed the next year by low-temperature single-molecule lifetime experiments for the canonical pentacene/p-terphenyl system.[147] The first room temperature studies observing the same molecule for an extended time were performed on R6G on surfaces using NSOM methods,[83,91,93] and a puzzling effect was reported that the observed lifetime depended upon the exact position of the tip with respect to the molecule. This turned out to be due to the quenching influence of the metallized portion of the tip on the molecular dipole emission. Later experiments have used far-field methods to avoid distortion of the observed lifetime.[92] In recent work, sophisticated data processing methods have been devised that allow one to dynamically shift the time frame over which the lifetime is measured, which allows observation of time-dependent changes in the lifetime due to dynamical quenching effects arising from conformational changes.[148] Single-molecule lifetime measurements have been useful in exploring tRNA dynamics,[149] DNA conformational fluctuations,[150] and electron transfer at interfaces,[151] to cite a selection of recent studies.

2. Single-molecule quantum optics

A further set of interesting time-dependent effects arises from the fact that the single molecule is a quantum-mechanical object, and hence quantum-optical correlations

are contained in the statistics of the photon emission times even for cw illumination. On the time scale of the excited state lifetime, photons emitted from single quantum system are expected to show photon antibunching, which means that the photons ''space themselves out in time,'' that is, the probability for two photons to arrive at the detector at the same time is small. Antibunching is fundamentally measured by computing the second-order correlation of the electric field $g^{(2)}(t)$ [which is simply the normalized form of the intensity-intensity correlation function $C_s(t)$], which shows a drop below the uncorrelated value of unity when antibunching is present.[152] For a single molecule, antibunching is easy to understand as the individual molecule cannot emit two photons at the same time. After photon emission, a time on the order of the inverse of the Rabi frequency must elapse before the probability of emission of a second photon is appreciable. At sufficiently high laser intensity, Rabi oscillations can be observed as the laser coherently drives the single molecule into and out of the excited state before emission occurs.

In actual practice, in order to overcome time limitations caused by the dead time of photomultipliers or SPADs, two identical detectors are used to measure the distribution of time delays between the arrival times of consecutive pairs of emitted photons as in the classical Hanbury Brown–Twiss experiment.[152] The expected antibunching in single-molecule emission was first observed for a single molecule of pentacene in p-terphenyl[153] demonstrating that quantum optics experiments can be performed in solids and for molecules. Of course, if more than one molecule is emitting, the antibunching effect as well as any bunching effect due to bottleneck states both quickly disappear since the various resonant molecules emit independently. The observation of high-contrast antibunching is strong proof that the spectral features are indeed those of single molecules. A variety of other quantum-optical experiments have been performed on single molecules at low temperatures, including ac Stark effects and electro-optical mixing, reviewed in Ref. 126.

In the room temperature regime, an extremely stable emitter is needed to complete useful single-molecule quantum optics experiments. For example, single CdSe/CdS nanocrystals show antibunching on the short (ns) time scale of the excited state lifetime,[59] in spite of serious blinking and fluctuation effects on longer time scales.[61] Surprisingly, researchers have shown that terrylene molecules protected from photo-oxidation in a p-terphenyl crystal at room temperature show a very low probability of photobleaching,[48] and this system showed clear high-contrast antibunching[154] under cw illumination.

Terrylene in p-terphenyl was recently utilized to produce a high efficiency, highly quantum mechanical source of single photons on demand.[155] A high performance, room temperature source of single photons at a designated repetition rate would be a key component in an optical quantum cryptography and communication system. It was possible to use a standard optical microscope and a simple doped molecular crystal to make a source in which the probability for single-photon emission per pump pulse was as large as 80%, a highly nonclassical value which strongly departs from the usual Poisson statistics. With this stable emitter, single photons could be emitted at a rate of several MHz for a total of 10^9 photons or more.

3. Intermediate time regime

In the time regime of microseconds to milliseconds, a large array of dynamical effects can be felt in the single-molecule emission, such as photophysical effects like intersystem crossing and photochemical effects such as protonation, electron transfer, or conformational fluctuations. Autocorrelation analysis has long been recognized as a useful method for statistical study of stochastic dynamical processes that may be partly obscured by noise.[23,156] By definition, the autocorrelation measures the similarity (overlap) between the photon emission signal $S(t)$ and a copy of $S(t)$ delayed in time by a lag time τ

$$C_S(\tau) = \int S(t)S(t+\tau)dt. \tag{13}$$

The shape of the autocorrelation function contains details of the dynamical process, under the assumption that the dynamical process is stationary, that is, the dynamics must not change during the time needed to record enough photon arrivals to generate a valid autocorrelation. Because the noise component of the signal is uncorrelated, its contribution to $C_s(t)$ decays quickly, leaving information about the (average) time-domain correlations of $S(t)$. In practice, when photon counting is used, a commercial digital correlator (Brookhaven, Malvern) is employed to measure $C_s(t)$ by keeping track of the arrival times of photons. Modern correlators can do this over a huge logarithmic time scale covering many decades in time, a feature that is very useful for studying the dispersive dynamics characteristic of amorphous systems.

It is important to distinguish two regimes: (a) measurement on the same single molecule for as long as possible, and (b) measurement of many single molecules, one at a time, but summing together the signals from all of them to increase the SNR of the correlation function. The latter regime is the FCS limit mentioned at the beginning of Sec. III, and FCS is generally performed for emitters at very low concentration in solution where diffusion is used to bring each new molecule into the volume to generate a new burst of emitted photons. The former regime is the primary focus of this article. The decay in the autocorrelation of the emitted photons for a single molecule of pentacene in p-terphenyl due triplet intersystem crossing effects was first reported in the low temperature studies,[3] and similar experiments in polymer systems allowed identification of different types of two-level systems in the host.[157]

4. Milliseconds and longer

Most single-molecule microscopy experiments explore the time scale from ms to many seconds, chiefly because the high intensity needed to obtain short-time information often results in premature bleaching. Moreover, most systems studied to date have shown some form of fluctuating, flickering, or stochastic behavior[6] arising from photochemistry, spectral

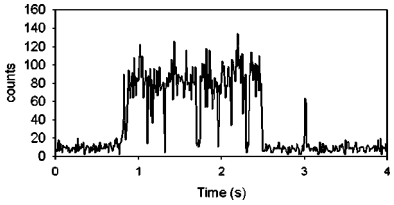

FIG. 11. Time trajectory of the emission from a single copy of the GFP mutant 10C in PAA using a confocal microscope, with 10 ms integration time and 514 nm pumping with an excitation intensity of 1.6 kW/cm^2 (from Ref. 109, used by permission).

shifts, enzymatic activity,[53] or environmental fluctuations between the chromophore and the surrounding host matrix. The full array of physical effects leading to fluctuations will not be reviewed here, but to give an example, Fig. 11 shows the time dependence of the photon emission signal for a single copy of a mutant GFP-even though the laser is on continuously throughout the trace, the emission from the single protein emitter turns on and off in a roughly digital fashion, but with several characteristic time scales.[109]

Fluctuating time-dependent signals like those shown in Fig. 11 may be analyzed in several ways. First of all, it is important to try to obtain as long a time trace with as many ''on/off'' switching events as possible to improve the statistical sample. If the time scale of interest is very long, then proper selection of the illumination duty cycle can be extremely helpful. With a sufficiently long time trace, calculation of the correlation function is a useful first step; if the process is characterized by simple two-state kinetics, the correlation function will be exponential. However, there are several single-molecule experiments where the decays are not simple single exponentials, indicating more complex kinetics.[149,158] One example would be the behavior of the angular orientation of single probe molecules in a polymer near the glass transition,[72] where stretched exponential kinetics have been observed. Another would be the dark time distributions of single CdSe quantum dots which show a power law time dependence.[61] In the event that the signal seems to switch between two values, experimenters generally attempt to extract separate distributions of on times and off times from the single-molecule time traces.[122] When this is possible, the experimenter can turn to the large array of mathematical analysis methods that have been previously developed for the analysis of single ion channel data.[14] As a further example at room temperature, correlation analysis has been applied to explore rotational correlations for molecules in polymers.[159]

For the case of single copies of the enzyme cholesterol oxidase, higher-order correlation analysis, in which the lengths of successive on-times were correlated, proved useful.[53,160] By this method, evidence was gathered for the hypothesis of fluctuating rate constants, an interesting type of dynamical disorder only observable at the single-molecule level.

V. DISCUSSION

This article has described in detail the experimental considerations and microscopic configurations needed to observe single-molecule fluorescence. The SNR depends upon a variety of properties of both the molecule of interest and the host matrix that should be carefully optimized. Microscope configurations of both the wide field and the scanning type can be used for such measurements. In all cases, the extraction of the maximum amount of information from each emitted photon is essential, and a variety of detection modalities are available. With the large array of successful techniques described here, it is to be expected that a further expansion of single-molecule optical measurements, unobscured by ensemble averaging, will occur.

ACKNOWLEDGMENTS

The authors thank W. P. Ambrose, S. Nishimura, M. Vrljic, and K. Willets for providing example data. This work has been supported in part by the National Science Foundation Grant Nos. 9816947 and 0212503. D. F. acknowledges the support of a NSF Graduate Fellowship.

[1] W. E. Moerner, AIP Conf. Proc. **323**, 467 (1995).
[2] W. E. Moerner and L. Kador, Phys. Rev. Lett. **62**, 2535 (1989).
[3] M. Orrit and J. Bernard, Phys. Rev. Lett. **65**, 2716 (1990).
[4] *Single Molecule Optical Detection, Imaging and Spectroscopy*, edited by T. Basché, W. E. Moerner, M. Orrit, and U. P. Wild (Verlag-Chemie, Munich, 1997).
[5] *Single Molecule Spectroscopy: Nobel Conference Lectures*, Springer Series Chem. Phys.; Vol. 67, edited by R. Rigler, M. Orrit, and T. Basché (Springer, Berlin, 2001).
[6] W. E. Moerner, Science **277**, 1059 (1997).
[7] J. C. Bergquist, R. G. Hulet, W. M. Itano, and D. J. Wineland, Phys. Rev. Lett. **57**, 1699–1702 (1986).
[8] Th. Basché, S. Kummer, and C. Bräuchle, Nature (London) **373**, 132 (1995).
[9] W. M. Itano, J. C. Bergquist, and D. J. Wineland, Science **237**, 612 (1987).
[10] F. Diedrich, J. Krause, G. Rempe, M. O. Scully, and H. Walther, IEEE J. Quantum Electron. **24**, 1314 (1988).
[11] H. Dehmelt, W. Paul, and N. F. Ramsey, Rev. Mod. Phys. **2**, 525 (1990).
[12] G. Binnig and H. Rohrer, Rev. Mod. Phys. **59**, 615 (1987).
[13] G. Binnig, C. F. Quate, and C. Gerber, Phys. Rev. Lett. **56**, 930 (1986).
[14] B. Sakmann and E. Neher, *Single Channel Recording* (Plenum, New York, 1995).
[15] T. T. Perkins, D. E. Smith, and S. Chu, Science **276**, 2016 (1997).
[16] S. M. Block, Cell **93**, 5 (1998).
[17] A. D. Mehta, M. Reif, J. A. Spudich, D. A. Smith, and R. M. Simmons, Science **283**, 1689 (1999).
[18] E. B. Shera, N. K. Seitzinger, L. M. Davis, R. A. Keller, and S. A. Soper, Chem. Phys. Lett. **174**, 553 (1990).
[19] C. W. Wilkerson, P. M. Goodwin, W. P. Ambrose, J. C. Martin, and R. A. Keller, Appl. Phys. Lett. **62**, 2030 (1993).
[20] S. Nie, D. T. Chiu, and R. N. Zare, Science **266**, 1018 (1994).
[21] W. P. Ambrose, A. M. Goodwin, J. H. Jett, A. VanOrden, J. H. Werner, and R. A. Keller, Chem. Rev. (Washington, D.C.) **99**, 2929–2956 (1999).
[22] *Single Molecule Detection in Solution*, edited by Ch. Zander, J. Enderlein, and R. A. Keller (Wiley, Berlin, 2002).
[23] D. L. Magde, E. L. Elson, and W. W. Webb, Biopolymers **13**, 29 (1974).
[24] M. Eigen and R. Rigler, Proc. Natl. Acad. Sci. U.S.A. **91**, 5740 (1994).
[25] R. Rigler, J. Biotechnol. **41**, 177 (1995).
[26] S. Maiti, U. Haupts, and W. W. Webb, Proc. Natl. Acad. Sci. U.S.A. **94**, 11753 (1997).
[27] P. Schwille, Cell Biochem. Biophys. **34**, 383 (2001).
[28] S. T. Hess, S. Huang, A. A. Heikal, and W. W. Webb, Biochemistry **41**, 607 (2002).
[29] *Fluorescence Correlation Spectroscopy*, Springer Series Chem. Phys., Vol. 65, edited by R. Rigler and E. Elson (Springer, Berlin, 2001).
[30] W. E. Moerner and Th. Basché, Angew. Chem., Int. Ed. Engl. **32**, 457 (1993).
[31] W. E. Moerner, Science **265**, 46 (1994).
[32] W. E. Moerner, Acc. Chem. Res. **29**, 563 (1996).

[33] M. Orrit, J. Bernard, R. Brown, and B. Lounis, in *Progress in Optics*, edited by E. Wolf (Elsevier, New York, 1996), Vol. 35, pp. 61–144.
[34] W. E. Moerner, R. M. Dickson, and D. J. Norris, Adv. At. Mol. Opt. Phys. **38**, 193 (1997).
[35] S. Nie and R. N. Zare, Annu. Rev. Biophys. Biomol. Struct. **26**, 567 (1997).
[36] T. Plakhotnik, E. A. Donley, and U. P. Wild, Annu. Rev. Phys. Chem. **48**, 181 (1996).
[37] X. S. Xie and J. K. Trautman, Annu. Rev. Phys. Chem. **49**, 441 (1998).
[38] W. E. Moerner and M. Orrit, Science **283**, 1670 (1999).
[39] S. Weiss, Science **283**, 1676 (1999).
[40] W. E. Moerner, J. Phys. Chem. B **106**, 910 (2002).
[41] A. M. Stoneham, Rev. Mod. Phys. **41**, 82 (1969).
[42] K. K. Rebane, *Impurity Spectra of Solids* (Plenum, New York, 1970).
[43] J. L. Skinner and W. E. Moerner, J. Phys. Chem. **100**, 13251 (1996).
[44] W. E. Moerner, J. Lumin. **60-1**, 997 (1994).
[45] T. Plakhotnik, W. E. Moerner, V. Palm, and U. P. Wild, Opt. Commun. **114**, 83 (1995).
[46] L. Kador, D. E. Horne, and W. E. Moerner, J. Phys. Chem. **94**, 1237 (1990).
[47] R. Y. Tsien and A. Waggoner, in *Handbook of Biological Confocal Microscopy*, 2nd ed., edited by J. B. Pawley (Plenum, New York, 1995), pp. 267–279.
[48] F. Kulzer, F. Koberling, T. Christ, A. Mews, and T. Basché, Chem. Phys. **247**, 23 (1999).
[49] C. Blum, F. Stracke, S. Becker, K. Mullen, and A. J. Meixner, J. Phys. Chem. A **105**, 6983 (2001).
[50] N. B. Bowden, K. A. Willets, W. E. Moerner, and R. M. Waymouth, Macromolecules **35**, 8122 (2002).
[51] G. S. Harms, L. Cognet, P. H. M. Lommerse, G. A. Blab, and T. Schmidt, Biophys. J. **80**, 2396 (2001).
[52] W. E. Moerner, J. Chem. Phys. **117**, 10925 (2002).
[53] H. P. Lu, L. Xun, and X. S. Xie, Science **282**, 1877 (1998).
[54] X. S. Xie and H. P. Lu, J. Biol. Chem. **274**, 15967 (1999).
[55] M. A. Bopp, Y. Jia, L. Li, R. J. Cogdell, and R. M. Hochstrasser, Proc. Natl. Acad. Sci. U.S.A. **94**, 10630 (1997).
[56] K. A. Willets, O. Ostroverkhova, M. He, R. J. Twieg, and W. E. Moerner, J. Am. Chem. Soc. **125**, 1174 (2003).
[57] S. Empedocles and M. Bawendi, Acc. Chem. Res. **32**, 389 (1999).
[58] M. J. Bruchez, M. Moronne, P. Gin, S. Weiss, and A. P. Alivisatos, Science **281**, 2013 (1998).
[59] B. L. Lounis, H. A. Bechtel, D. Gerion, P. Alivisatos, and W. E. Moerner, Chem. Phys. Lett. **329**, 399 (2000).
[60] M. Nirmal, B. O. Dabbousi, M. G. Bawendi, J. J. Macklin, J. K. Trautman, T. D. Harris, and L. E. Brus, Nature (London) **383**, 802 (1996).
[61] M. Kuno, D. P. Fromm, H. F. Hamann, A. Gallagher, and D. J. Nesbitt, J. Chem. Phys. **112**, 3117 (2000).
[62] K. K. Rebane, Chem. Phys. **189**, 139 (1994).
[63] R. J. Silbey and R. A. Alberty, *Physical Chemistry*, 3rd ed. (Wiley, New York, 2001).
[64] K. K. Rebane and I. Rebane, J. Lumin. **56**, 39 (1993).
[65] S. A. Soper, H. L. Nutter, R. A. Keller, L. M. Davis, and E. B. Shera, Photochem. Photobiol. **57**, 972 (1993).
[66] W. P. Ambrose, Th. Basché, and W. E. Moerner, J. Chem. Phys. **95**, 7150 (1991).
[67] H. de Vries and D. A. Wiersma, J. Chem. Phys. **72**, 1851 (1980).
[68] W. E. Moerner, A. R. Chraplyvy, and A. J. Sievers, Phys. Rev. B **29**, 6694 (1984).
[69] T. Schmidt, Single Molecules **2**, 217 (2001).
[70] A. H. Iwane, T. Funatsu, Y. Harada, M. Tokunaga, O. Ohara, S. Morimoto, and T. Yanagida, FEBS Lett. **407**, 235 (1997).
[71] R. Yasuda, H. Noji, K. Kinosita, and M. Yoshida, Cell **93**, 1117 (1998).
[72] L. A. Deschenes and D. A. Vanden Bout, Science **292**, 255 (2001).
[73] K. D. Weston, P. J. Carson, J. A. DeAro, and S. K. Buratto, Chem. Phys. Lett. **308**, 58 (1999).
[74] Th. Basché, W. P. Ambrose, and W. E. Moerner, J. Opt. Soc. Am. B **9**, 829 (1992).
[75] E. H. Hellen and D. Axelrod, J. Opt. Soc. Am. B **4**, 337 (1987).
[76] E. Betzig and R. J. Chichester, Science **262**, 1422 (1993).
[77] E. B. Shera, N. K. Seitzinger, L. M. Davis, R. A. Keller, and S. A. Soper, Chem. Phys. Lett. **174**, 553 (1990).
[78] L.-A. Li and L. Davis, Rev. Sci. Instrum. **64**, 1524 (1993).
[79] M. Unger, E. Kartalov, C. S. Chiu, H. A. Lester, and S. R. Quake, Biotechniques **27**, 1008 (1999).
[80] P. Tchénio, A. B. Myers, and W. E. Moerner, J. Phys. Chem. **97**, 2491 (1993).
[81] P. Tchénio, A. B. Myers, and W. E. Moerner, Chem. Phys. Lett. **213**, 325 (1993).
[82] A. B. Myers, P. Tchénio, M. Zgierski, and W. E. Moerner, J. Phys. Chem. **98**, 10377 (1994).
[83] J. K. Trautman, J. J. Macklin, L. E. Brus, and E. Betzig, Nature (London) **369**, 40 (1994).
[84] H. Peter Lu and X. S. Xie, Nature (London) **385**, 143 (1997).
[85] M Born and E Wolf, *Principles of Optics* (Cambridge University Press, Cambridge, 1999).
[86] T. R. Corle and G. S. Kino, *Confocal Scanning Optical Microscopy and Related Imaging Systems* (Academic, San Diego, 1996).
[87] J. K. Trautman and W. P. Ambrose, in *Single-Molecule Optical Detection, Imaging, and Spectroscopy*, edited by T. Basché *et al.* (VCH, Weinheim, 1997).
[88] E. Betzig, J. K. Trautman, T. D. Harris, J. S. Weiner, and R. K. Kostelak, Science **251**, 146 (1991).
[89] B. Hecht, B. Sick, U. P. Wild, V. Decker, R. Zenobi, O. J. F. Martin, and D. W. Pohl, J. Chem. Phys. **112**, 7761 (2000).
[90] E. Betzig and R. J. Chichester, Science **262**, 1422 (1993).
[91] W. P. Ambrose, P. M. Goodwin, J. C. Martin, and R. A. Keller, Science **265**, 364 (1994).
[92] J. K. Trautman and J. J. Macklin, Chem. Phys. **205**, 221 (1996).
[93] X. S. Xie and R. C. Dunn, Science **265**, 361 (1994).
[94] X. S. Xie, Acc. Chem. Res. **29**, 598 (1996).
[95] F. Zenhausern, Y. Martin, and H. K. Wickramasinghe, Science **269**, 1083 (1995).
[96] H. F. Hamann, A. Gallagher, and D. J. Nesbitt, Appl. Phys. Lett. **73**, 1469 (1998).
[97] E. J. Sanchez, L. Novotny, and X. S. Xie, Phys. Rev. Lett. **82**, 4014 (1999).
[98] H. F. Hamann, M. Kuno, A. Gallagher, and D. J. Nesbitt, J. Chem. Phys. **114**, 8596 (2001).
[99] T. W. Klar and S. W. Hell, Opt. Lett. **24**, 954 (1999).
[100] E. Betzig, Opt. Lett. **20**, 237 (1995).
[101] T. Funatsu, Y. Harada, M. Tokunaga, K. Saito, and T. Yanagida, Nature (London) **374**, 555 (1995).
[102] G. J. Schütz, G. Kada, V. P. Pastushenko, and H. Schindler, EMBO J. **19**, 892 (2000).
[103] M. Vrjlic, S. Y. Nishimura, S. Brasselet, W. E. Moerner, and H. M. McConnell, Biophys. J. **83**, 2681 (2002).
[104] D. Axelrod, T. P. Burghardt, and N. L. Thompson, Annu. Rev. Biophys. Bioeng. **13**, 247 (1984).
[105] N. L. Thompson, H. M. McConnell, and T. P. Burghardt, Biophys. J. **46**, 739 (1984).
[106] R. M. Dickson, D. J. Norris, Y.-L. Tzeng, and W. E. Moerner, Science **274**, 966 (1996).
[107] R. M. Dickson, A. B. Cubitt, R. Y. Tsien, and W. E. Moerner, Nature (London) **388**, 355 (1997).
[108] S. Kummer, R. M. Dickson, and W. E. Moerner, Proc. Soc. Photo-Opt. Instrum. Eng. **3273**, 165 (1998).
[109] W. E. Moerner, E. J. G. Peterman, S. Brasselet, S. Kummer, and R. M. Dickson, Cytometry **36**, 232 (1999).
[110] M. F. Paige, E. J. Bjerneld, and W. E. Moerner, Single Molecules **2**, 191 (2001).
[111] Y. Sako, S. Minoghchi, and T. Yanagida, Nat. Cell Biol. **2**, 168 (2000).
[112] W. P. Ambrose, P. M. Goodwin, and J. P. Nolan, Cytometry **36**, 224 (1999).
[113] Th. Schmidt, G. J. Schutz, W. Baumgartner, H. J. Gruber, and H. Schindler, Proc. Natl. Acad. Sci. U.S.A. **93**, 2926 (1996).
[114] T. Ha, T. A. Laurence, D. S. Chemla, and S. Weiss, J. Phys. Chem. B **103**, 6839 (1999).
[115] J. N. Forkey, M. E. Quinlan, and Y. E. Goldman, Prog. Biophys. Mol. Biol. **74**, 1 (2000).
[116] T. Ha, T. Enderle, D. S. Chemla, P. R. Selvin, and S. Weiss, Phys. Rev. Lett. **77**, 3979 (1996).
[117] K. D. Weston and L. S. Goldner, J. Phys. Chem. B **105**, 3453 (2001).
[118] T. Ha, J. Glass, T. Enderle, D. S. Chemla, and S. Weiss, Phys. Rev. Lett. **80**, 2093 (1998).
[119] K. Adachi, R. Yasuda, H. Noji, H. Itoh, Y. Harada, M. Yoshida, and K. Kinosita, Proc. Natl. Acad. Sci. U.S.A. **97**, 7243 (2000).

[120] H. Sosa, E. J. G. Peterman, W. E. Moerner, and L. S. B. Goldstein, Nat. Struct. Biol. **8**, 540 (2001).
[121] E. J. G. Peterman, H. Sosa, L. S. B. Goldstein, and W. E. Moerner, Biophys. J. **81**, 2851 (2001).
[122] E. J. G. Peterman, S. Brasselet, and W. E. Moerner, J. Phys. Chem. A **103**, 10553 (1999).
[123] R. M. Dickson, D. J. Norris, and W. E. Moerner, Phys. Rev. Lett. **81**, 5322 (1998).
[124] B. Sick, B. Hecht, and L. Novotny, Phys. Rev. Lett. **85**, 4482 (2000).
[125] J. T. Fourkas, Opt. Lett. **26**, 211 (2001).
[126] Ph. Tamarat, A. Maali, B. L. Lounis, and M. Orrit, J. Phys. Chem. A **104**, 1 (2000).
[127] L. Fleury, P. Tamarat, B. Lounis, J. Bernard, and M. Orrit, Chem. Phys. Lett. **236**, 87 (1995).
[128] D. A. Vanden Bout, W. T. Yip, D. Hu, D. K. Fu, T. M. Swager, and P. F. Barbara, Science **277**, 1074 (1997).
[129] Y. Hou, A, M. Bardo, C. Martinez, and D. A. Higgins, J. Phys. Chem. B **104**, 212 (2000).
[130] B. W. Van der Meer, G. Coker III, and S.-Y. Chen, *Resonance Energy Transfer: Theory and Data* (VCH, New York, 1994).
[131] R. M. Clegg, in *Fluorescence Imaging Spectroscopy and Microscopy*, edited by X. F. Wang and B. Herman (Wiley, New York, 1996), Vol. 137, pp. 179–252.
[132] J. R. Lakowicz, *Principles of Fluorescence Spectroscopy* (Kluwer Academic, New York, 1999).
[133] T. Ha, Methods **25**, 78 (2001).
[134] L. Stryer, Annu. Rev. Biochem. **47**, 819 (1978).
[135] T. Ha, X. Zhuang, H. D. Kim, J. W. Orr, J. R. Williamson, and S. Chu, Proc. Natl. Acad. Sci. U.S.A. **96**, 9077 (1999).
[136] A. N. Kapanidis and S. Weiss, J. Chem. Phys. **117**, 10953 (2002).
[137] S. Brasselet, E. J. G. Peterman, A. Miyawaki, and W. E. Moerner, J. Phys. Chem. B **104**, 3676 (2000).
[138] A. Miyawaki, J. Llopis, R. Heim, J. M. McCaffrey, J. A. Adams, M. Ikura, and R. Y. Tsien, Nature (London) **388**, 882 (1997).
[139] T. Ha, A. Y. Ting, J. Liang, W. B. Caldwell, A. A. Deniz, D. S. Chemla, P. G. Schultz, and S. Weiss, Proc. Natl. Acad. Sci. U.S.A. **96**, 893 (1999).
[140] X. Zhuang, L. Bartley, H. Babcock, R. Russell, T. Ha, D. Herschlag, and S. Chu, Science **288**, 2048 (2000).
[141] Y. Jia, D. S. Talaga, W. L. Lau, H. S. M. Lu, W. F. DeGrado, and R. M. Hochstrasser, Chem. Phys. **247**, 69 (1999).
[142] T. Ha, I. Rasnik, W. Cheng, H. P. Babcock, G. H. Gauss, T. M. Lohman, and S. Chu, Nature (London) **419**, 638 (2002).
[143] W. Denk, J. H. Strickler, and W. W. Webb, Science **248**, 73 (1990).
[144] J. Mertz, C. Xu, and W. W. Webb, Opt. Lett. **20**, 2532 (1995).
[145] E. J. Sanchez, L. Novotny, G. R. Holtom, and X. S. Xie, J. Phys. Chem. A **101**, 7019 (1997).
[146] S. A. Soper, L. M. Davis, and E. B. Shera, J. Opt. Soc. Am. B **9**, 1761 (1992).
[147] M. Pirotta, F. Güttler, H. Gygax, A. Renn, J. Sepiol, and U. P. Wild, Chem. Phys. Lett. **208**, 379 (1993).
[148] C. Eggeling, J. R. Fries, L. Brand, R. Gunther, and C. A. M. Seidel, Proc. Natl. Acad. Sci. U.S.A. **95**, 1556 (1998).
[149] Y. Jia, A. Sytnik, L. Li, S. Vladimarov, B. S. Cooperman, and R. M. Hochstrasser, Proc. Natl. Acad. Sci. U.S.A. **94**, 7932 (1997).
[150] S. Wennmalm, L. Edman, and R. Rigler, Chem. Phys. **247**, 61 (1999).
[151] H. P. Lu and X. S. Xie, J. Phys. Chem. B **101**, 2753 (1997).
[152] R. Loudon, *The Quantum Theory of Light*, 2nd ed. (Clarendon, Oxford, 1983).
[153] Th. Basché, W. E. Moerner, M. Orrit, and H. Talon, Phys. Rev. Lett. **69**, 1516 (1992).
[154] L. Fleury, J.-M. Segura, G. Zumofen, B. Hecht, and U. P. Wild, Phys. Rev. Lett. **84**, 1148 (2000).
[155] B. Lounis and W. E. Moerner, Nature (London) **407**, 491 (2000).
[156] E. L. Elson and D. Magde, Biopolymers **13**, 1 (1974).
[157] A. Zumbusch, L. Fleury, R. Brown, J. Bernard, and M. Orrit, Phys. Rev. Lett. **70**, 3584 (1993).
[158] L. Edman and R. Rigler, Proc. Natl. Acad. Sci. U.S.A. **97**, 8266 (2000).
[159] A. P. Bartko and R. M. Dickson, J. Phys. Chem. B **103**, 3053 (1999).
[160] G. K. Schenter, H. P. Lu, and X. S. Xie, J. Phys. Chem. A **103**, 10477 (1999).